

# The H<sub>I</sub> Distribution of the Milky Way

Peter M.W. Kalberla and Jürgen Kerp

Argelander-Institut für Astronomie, Universität Bonn, D-53012 Bonn, Germany;  
email: pkalberla@astro.uni-bonn.de, jkerp@astro.uni-bonn.de

Annu. Rev. Astron. Astrophys. 2009. 47:27–61

The *Annual Review of Astronomy and Astrophysics* is online at [astro.annualreviews.org](http://astro.annualreviews.org)

This article's doi:  
10.1146/annurev-astro-082708-101823

Copyright © 2009 by Annual Reviews.  
All rights reserved

0066-4146/09/0922-0027\$20.00

## Key Words

21-cm line surveys, disk, halo, Galactic structure, interstellar medium

## Abstract

Neutral atomic hydrogen (H<sub>I</sub>) traces the interstellar medium (ISM) over a broad range of physical conditions. Its 21-cm emission line is a key probe of the structure and dynamics of the Milky Way Galaxy. About 50 years after the first detection of the 21-cm line the exploration of the H<sub>I</sub> distribution of the Milky Way has undergone a true renaissance. This was triggered by several large-scale 21-cm surveys that became available within the past decade. New all-sky surveys unravel the shape and volume density distribution of the gaseous disk up to its borders. High-resolution Galactic plane surveys disclose a wealth of shells, filaments, and spurs that bear witness to the recycling of matter between stars and the ISM. All these observational results indicate that the H<sub>I</sub> gas traces a dynamical Galactic ISM with structures on all scales, from tens of astronomical units to kiloparsecs. The Galaxy can be considered to be a violent, breathing disk surrounded by highly turbulent extra-planar gas.

---

**ISM:** interstellar medium

---

## 1. INTRODUCTION

To characterize the H I distribution of the Milky Way one needs to cover many different aspects and it is nearly impossible to compile a comprehensive view within a single review. Excellent reviews have been written by Kulkarni & Heiles (1987, 1988), Burton (1976, 1988, 1992), Dickey & Lockman (1990), and Dickey (2002). We do not try to compile all the fundamental aspects published there but want to provide a comprehensive overview on observational improvements and major results of the past decade. This review does not intend to give an encyclopedic bibliography on the earlier science. The reader will find these references in earlier reviews and other papers mentioned here.

Several major surveys have been released during the past decade and the data are accessible for public use. All surveys provide unbiased databases across large coherent regions. Significant efforts went into improvements in sensitivity, dynamic range, velocity coverage and data quality (reducing the imprint of systematic effects). All-sky surveys like the Leiden-Dwingeloo survey (LDS, Hartmann & Burton 1997), the Instituto Argentino de Radioastronomía survey (IAR, Bajaja et al. 2005), and the combined Leiden-Argentine-Bonn survey (LAB, Kalberla et al. 2005) provide general-purpose databases, particularly suitable for the analysis of large-scale phenomena. Their major limitation is due to the beam-by-beam grid with an angular resolution of  $\sim 36$  arcmin. Interferometric Galactic plane surveys like the Canadian Galactic Plane Survey (CGPS, Taylor et al. 2003), the Southern Galactic Plane Survey (SGPS, McClure-Griffiths et al. 2005), and the VLA Galactic Plane Survey (VGPS, Stil et al. 2006b) offer much higher angular resolution of about 1 arcmin, but are restricted to a few degrees in Galactic latitude only. Their modest sensitivity of a few Kelvin (one or two orders of magnitude worse than single-dish work) implies, for many of the scientific problems focused upon in this manuscript, that the single-dish data are more appropriate.

Multifeed arrays in foci of large single-dish telescopes reduce the survey duration proportional to the number of feeds used. Today it is feasible to perform all-sky surveys with excellent sensitivity on a fully sampled angular grid within about two years of observations. The Arecibo Galactic ALFA survey aims to cover both the Galactic plane and the high-latitude sky with a 3.4 arcmin resolution, in total about 30% of the whole sky (GALFA-H I; Stanimirović et al. 2006). The Parkes Galactic All-Sky Survey (GASS) covers the whole Southern Hemisphere with 16 arcmin resolution (McClure-Griffiths et al. 2009). The Effelsberg-Bonn H I Survey (EBHIS, Winkel et al. 2008) will complement the northern sky with an angular resolution of 9 arcmin. Parallel to the development of multifeed front-ends, a revolution took place for spectrometer backends. Field-Programmable-Gate-Array (FPGA) spectrometers offer large bandwidths, high-dynamic ranges, and spectra-storage times of less than a second. The latter is of high importance to mitigate the Radio-Frequency-Interference (RFI) signals that pollute the line emission even within the protected 21-cm line band.

We focus on scientific research areas that benefit from this technological progress:

- The global picture of the H I distribution in the Milky Way (a quasi-static view, large scales),
- The violent interstellar medium (ISM) (a dynamical view, small scales), and
- H I as part of the multiphase structure of the ISM (the physical state of the H I distribution).

Properties of the large-scale H I distribution in the Milky Way can be derived best from the LAB survey. We discuss this first with the caveat that most of the derived parameters depend on the adopted Galactic rotation curve. At present, there appears to exist a general consensus that a flat rotation curve with  $v_{\text{rot}} \sim 220 \text{ km s}^{-1}$  is most likely, so we use this approximation. A derivation of the gas distribution inside the solar circle is ambiguous, but for Galactocentric radii  $R \gtrsim R_{\odot}$  one gets on average an exponential distribution of the H I surface density with a radial scale length

of  $R_c = 3.75$  kpc. The gaseous disk is strongly warped, up to  $\sim 5$  kpc in the north, but the bending of the mid-plane is well defined with three basic Fourier modes for  $R \lesssim 40$  kpc.

The gaseous disk flares strongly. The scale height of the H I gas layer increases exponentially with  $R$ ; at the same time the mid-plane volume density and the surface density fall off exponentially. There is a tight correlation between surface density, mid-plane volume density, and scale height for  $R \lesssim 35$  kpc. Spiral structures are observable to the same distance; they cause fluctuations in density and scale height. This suggests that the H I disk of the Milky Way is well defined out to  $R \sim 35$  kpc. At larger radial distances the Milky Way is surrounded by a faint, patchy, and highly turbulent H I distribution that has been traced out to  $R \sim 60$  kpc (Kalberla & Dedes 2008).

The global H I density distribution suggests that in total about 10% of the H I gas is “anomalous” in the sense that it stands out from the main gas layer. Many aspects of this anomalous population can be reproduced by modeling a distribution of clumps with a turbulent velocity dispersion of  $\sigma \sim 74$  km s<sup>-1</sup>. This H I gas floats around at large  $z$  distances, up to several scale heights above the disk. This extraplanar gas layer appears to be approximately corotating with the disk, but somewhat lagging behind. The vertical gradient in the rotation velocity appears to depend predominantly on the scale height of individual gas components. A large fraction of this gas is cold and clumpy on parsec scales, probing the conditions in the lower Galactic halo.

The H I disk shows small-scale structure on all scales. H I filaments may reach altitudes of several kiloparsecs. The Galactic plane surveys, in particular, disclose a wealth of shells, spurs, and chimneys. These structures are the most prominent tracers of the Galactic “ecosystem.” Shells are found to be concentrated at mid-plane, and 50% of them at  $z \lesssim 500$  pc. About 5% of the disk volume appears to be occupied by shells. The radial distribution has an exponential scale length of  $\sigma_{shell} = 3_{-1}^{+2}$  kpc, which is comparable to the scale length of the stellar disk. Individual supernovae trigger violent interactions that throw the ISM locally out of balance. At the same time, collective effects lead to a dynamical equilibrium between the different phases of the ISM.

The H I gas has a two-phase structure, characterized by the cold neutral medium (CNM), which has a cloudy structure, and the warm neutral medium (WNM) with a diffuse distribution. In the classical two-phase picture, both phases exist in pressure equilibrium with stable phases for temperatures of  $T \lesssim 300$  K (CNM) and  $T \gtrsim 5000$  K (WNM) embedded in a hot ionized phase (McKee & Ostriker 1977). Gas at intermediate temperatures is considered to be transient. We discuss the properties of these H I phases in detail, in particular, characteristic timescales for both phases, which differ by two orders of magnitude. The typical cooling time for the CNM is  $\sim 1.4 \times 10^5$  years, in comparison to  $\sim 5 \times 10^7$  years for the WNM. In the presence of a highly dynamical ISM, this implies severe constraints for any equilibrium considerations. Shocks due to supernovae are expected to occur every  $\sim 5 \times 10^6$  years; in such cases, the WNM has hardly sufficient time to relax.

Investigations by Wolfire et al. (2003) predict for the H I gas two phases in the disk out to  $R \lesssim 18$  kpc, but also gas injected into the halo by a Galactic fountain may have this structure up to heights of several kiloparsecs above the disk. Numerical simulations of thermal instabilities in a turbulent flow suggest that turbulence can enhance phase transitions over a broad range of temperatures, consistent with the finding that 50% of the gas in the disk is observed in the unstable range  $300 \lesssim T \lesssim 5000$  K (Gazol et al. 2001). Turbulence is also found to generate density perturbations on small scales, enhancing thermal instabilities in this way.

Cold H I structures have been observed on scales of parsecs down to tens of astronomical units against continuum background sources. Predominantly within the Galactic plane H I self-absorption (HISA) features against the extended line background of the WNM have been found. CNM clouds have typical temperatures in the range of 40 to 100 K, with a median temperature of about 60 K. Turbulence may also explain why a large fraction of the extraplanar gas is

---

**CNM:** cold neutral medium  
**WNM:** warm neutral medium  
**HISA:** H I self-absorption

---

---

**HVC:** high-velocity cloud

**HIM:** hot ionized medium

---

cold and clumpy. The same argument may apply to high-velocity clouds (HVCs). Their specific turbulent-energy densities are an order of magnitude larger than that of comparable disk material. Accordingly it is no surprise that most of the HVC complexes show two phases in H $\alpha$ . There is mounting evidence that H $\alpha$  HVCs are embedded in a hot ionized medium (HIM,  $10^{6.15}$  K) and surrounded by a highly ionized interface. Because the HIM is bound to the Milky Way, this may imply that many, if not most, of the HVCs are associated with the Milky Way.

## 2. INSTRUMENTS, OBSERVATIONS, AND STRATEGIES

### 2.1. Surveys

About 90% of the H $\alpha$  mass is localized within a rather well-defined thin disk; a detailed discussion of its properties is given in Section 3. The Sun is embedded within this disk in such a way that there is no single line of sight across the whole sky without H $\alpha$  gas emission. The observed column densities vary across the sky by a factor of about 100. H $\alpha$  in the Galactic plane shows up with column density fluctuations of an order of magnitude on angular scales of a few arcmin. The full width at half maximum (FWHM) line width of H $\alpha$  clouds can be, in extreme cases, as narrow as  $1 \text{ km s}^{-1}$ , indicating gas temperatures of 20 K (Knapp & Verschuur 1972). But such narrow structures are rarely observed toward the high Galactic latitude sky and are associated with the infrared cirrus (Low et al. 1984). At high latitudes most of the H $\alpha$  21-cm emission lines at low velocities are broad, indicating a high degree of turbulence and gas temperatures in excess of a few thousand Kelvin.

We need accordingly different observing strategies to investigate the physical conditions of the ISM traced by the H $\alpha$  21-cm line. Toward the Galactic plane, observations with high angular and spectral resolution are required; interferometers are ideally suited to resolve the spatial structure but they are today still limited by the number of spectral channels and sensitivity. At present, the on-board processing power of the correlator constrains the number of spectral channels and the usable bandwidth of the observations. Moreover, radio interferometers are inherently non-sensitive for the associated faint and diffusely distributed emission of the WNM. This obvious limitation can be overcome by adding the “missing short spacings” from single-dish observations (Section 2.2.3).

Toward high Galactic latitudes we can study most of the gas properties with moderate angular resolution but high sensitivity. For these purposes, single-dish telescopes are ideally suited because they offer moderate angular, highest spectral resolution and high sensitivity to reach brightness temperature limits down to a few mK. However, to quantify such faint emission the single-dish data have to be corrected for several systematic effects. Most important are RFI rejection and the correction for the so-called stray radiation (Section 2.2.2).

In the following we discuss briefly large-scale surveys performed with single-dish telescopes and radio interferometers available today; **Figure 1** shows the sky coverages of these surveys.

**2.1.1. Full-sky surveys.** As a general-purpose database the LAB survey (Kalberla et al. 2005) with an angular resolution of 36 arcmin sampled on a beam-by-beam grid and a velocity resolution of  $1 \text{ km s}^{-1}$  is available. This survey combines the IAR southern sky survey (Bajaja et al. 2005) with a version of the LDS (Hartmann & Burton 1997) to which a refined stray radiation correction had been applied. This refinement was possible when the IAR data became available to augment the input sky necessary for modeling the correction, including also corrections for reflections from the ground, and led to improvement of the correction originally applied by Hartmann et al. (1996). Currently, this is the most sensitive Milky Way 21-cm line survey with the most extensive coverage

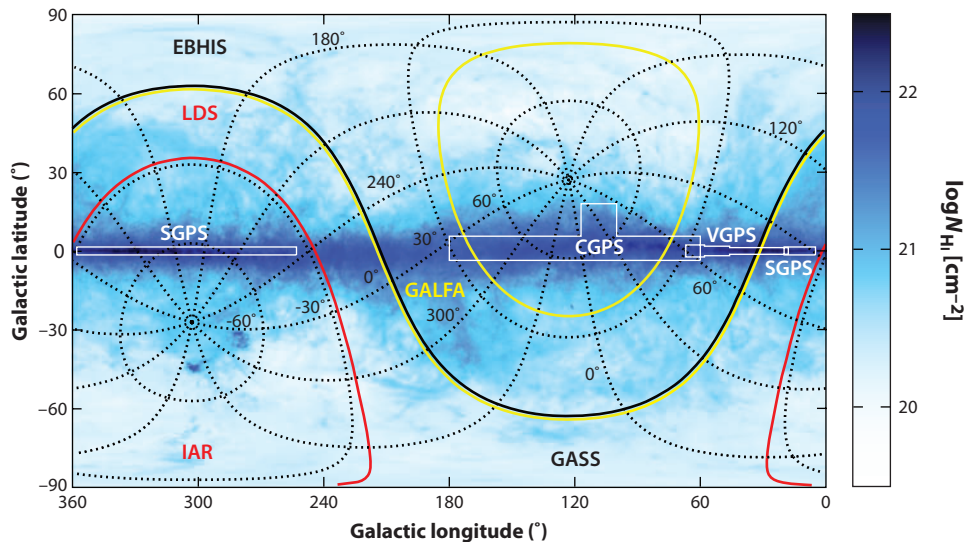


**Figure 1**

Overview of the sky coverage of different surveys. The Leiden-Argentine-Bonn (LAB) survey merges the Leiden-Dwingeloo Survey and Instituto Argentino de Radioastronomía surveys at  $\delta = -27.5^\circ \pm 2.5^\circ$  (red line). The Galactic All-Sky Survey and Effelsberg-Bonn HI Survey cover the northern and southern sky, separated by the black line. The Arcicbo Galactic ALFA survey coverage is  $-2^\circ < \delta < +38^\circ$  (yellow lines). The Galactic plane survey consists of Southern Galactic Plane Survey, Canadian Galactic Plane Survey, and VLA Galactic Plane Survey. The background image displays the total volume density of the 21-cm line emission from the LAB survey. This figure was kindly provided by B. Winkel.

both spatially and kinematically ( $-450 \lesssim v_{lsr} \lesssim 400 \text{ km s}^{-1}$ ). The sensitivity reaches the 70- to 90-mK level, and remaining baseline uncertainties are at a level of 20 to 40 mK. 3-D data cubes are available at CDS, and an easy to use interface to access individual spectra and column densities is provided by [http://www.astro.uni-bonn.de/~webrai/english/tools\\_labsurvey.php](http://www.astro.uni-bonn.de/~webrai/english/tools_labsurvey.php).

**2.1.2. Radio Interferometer Galactic Plane Surveys.** The International Galactic Plane Survey (IGPS) comprises many radio telescope surveys to map the ISM in the Galactic plane at various wavelengths. Contributions at the 21-cm line are from the CGPS by Taylor et al. (2003), the SGPS by McClure-Griffiths et al. (2005), and the VGPS by Stil et al. (2006b). These surveys provide 21-cm line data with an angular resolution of 1–3.3 arcmin. Unfortunately, the sensitivity is limited ( $\sim 2 \text{ K}$ ). The IGPS is still an ongoing project; for data access and detailed information on all of these surveys we refer to <http://www.ras.ucalgary.ca/IGPS/>.

**2.1.3. Multifield single-dish surveys.** The LAB all-sky survey provides data with excellent sensitivity; but for those parts of the Galactic sky without interferometric data, the angular resolution is seriously limited. The IGPS, however, is rather restricted in Galactic latitude coverage and sensitivity. With the advent of multifield receivers, it became possible to use the world’s largest single-dish telescopes to perform all-sky surveys in a very efficient way, providing data with improved sensitivity and resolution; it was an important improvement over currently available single-dish or interferometer surveys.

The Parkes telescope, equipped with 13 feeds, was used to map the HI in the southern sky with a sensitivity of 60 mK (McClure-Griffiths et al. 2009) and the angular resolution

was 16 arcmin. The first release of a stray-radiation-corrected version is expected for 2009 (<http://www.atnf.csiro.au/research/GASS/>).

The Arecibo telescope, equipped with a seven-beam Arecibo L-band Feed Array (ALFA), is currently used for Galactic studies for the declination range  $-2^\circ < \delta < +38^\circ$ . Focusing on the Milky Way radiation, the GALFA-HI survey aims to cover both the Galactic plane and high latitudes with an excellent angular resolution of 3.4 arcmin [see <http://www.naic.edu/alfa/galfa>; see also Stanimirović et al. 2006 (GALFA-HI)].

A complete survey of the northern sky commenced in autumn 2008 with the seven-beam receiver of the 100-m telescope (EBHIS). The sky north of declination  $\delta = 0^\circ$  will be mapped on a fully sampled grid with an angular resolution of 9 arcmin (Winkel et al. 2008). Using state-of-the-art FPGA spectrometers (Section 2.2.4), it is feasible to observe the Milky Way emission with velocity resolution of  $\sim 1.3 \text{ km s}^{-1}$  and external galaxies with redshifts of  $z \leq 0.07$  at the same time.

## 2.2. New Observational Techniques

**2.2.1. Multifield receiver systems.** Already about thirty years ago, large full steerable radio telescopes approached technological limits in size and weight. The special design of the Green Bank telescope with an unblocked aperture led to some additional improvements, but a major innovation came from multifield receiver systems. For single-dish telescopes multifield receivers offer the opportunity to improve the survey speed by up to an order of magnitude.

The Parkes Telescope was the first with a 13-feed array at 1.4 GHz (Staveley-Smith 1997), followed by the Arecibo 300-m dish, which is now equipped with a seven-beam receiver system. Using this device, several international research collaborations were successfully established to perform unique observations on the highest signal-to-noise ratio in the Galactic (GALFA-HI, Stanimirović et al. 2006), extragalactic (EALFA, Giovanelli 2008), and pulsar (PALFA, Cordes et al. 2006) research. Also in 2008, the Effelsberg 100-m dish got equipped with a seven-beam receiver system. With these receivers, all these telescopes realized a major leap in observing efficiency.

Current multifield systems undersample the focal plane. Focal-plane phased-arrays will overcome this limitation in the near future. Single-dish telescopes would benefit from another major increase of the survey speed (Giovanelli 2008) and interferometers from a significant enlargement of the instantaneous field of view (Verheijen et al. 2008). Current activities at CSIRO and DRAO are summarized by Johnston et al. (2007).

**2.2.2. Stray radiation mitigation strategies.** Up to 50% of the HI emission lines observed at regions of low total HI flux with single-dish telescopes may be spurious, picked up by far-off antenna side-lobes from the bright Galactic plane (e.g., figure 14 of Hartmann et al. 1996). This stray radiation problem is caused by reflections within the telescope, mainly at the feed support legs, but also at the rim of the reflector, the spill-over region. Even reflections from the ground are present. Stray radiation is most serious in regions with faint HI emission received by the main beam, but also for HI observations of the Galactic plane, stray radiation cannot be neglected entirely if we are interested in faint lines associated with large velocity dispersion. For an accurate evaluation of the faint and extended emission toward high latitudes, a correction of all these spurious effects is necessary (Kalberla, Mebold & Reich 1980).

Stray radiation is not entirely avoidable. The Robert C. Byrd Green Bank Telescope (GBT) is a prime example of a new telescope design with an unblocked aperture. This improves the aperture efficiency and minimizes baseline ripples caused by standing waves. Most of the stray radiation is mitigated, in particular that from the support legs (Dickey & Lockman 1990), but the spillover may

still cause problems (Lockman & Condon 2005). A correction without the knowledge of the beam pattern requires bootstrapping from a database that is unaffected by stray radiation (Lockman, Jahoda & McCammon 1986); the LAB survey can be used for this purpose.

Alternatively, it is feasible to calculate the bias introduced by stray radiation. In this case, it is necessary to measure or model the antenna diagram as accurately as possible. The stray radiation can be removed by convolving the observed all-sky 21-cm line emission (i.e., LAB survey) with the antenna diagram. This became a standard procedure for the Effelsberg 100-m telescope and has been successfully applied to the full sky (Higgs & Tapping 2000, Kalberla et al. 2005). The corrected data reveal a quality that is equivalent to a main beam efficiency of 99%.

**2.2.3. Short-spacing correction.** Radio interferometers are insensitive to extended structures because they do not receive emission from spatial frequencies shorter than the smallest separation of two telescopes of the telescope array. For observations of the Galactic HI emission, this property causes serious problems because a significant fraction of the HI emission is extended on scales of tens of arcminutes, corresponding to the shortest interferometer spacings. As a result, the total flux is undefined, most of the WNM remains unobservable, and even some parts of the CNM may get suppressed in interferometer maps. Restoration methods like CLEAN (see Högbom 1974) fail because the Galactic HI can in general not be approximated by a superposition of point sources. The missing information needs to be filled in and this is possible if one uses a single-dish telescope with a diameter of at least 1.5 times the shortest interferometer baseline. This procedure is called short-spacing correction; the resulting data are equivalent to observations with a virtual single-dish telescope having a diameter of 500 m or more.

There are different methods available. For a comparison and useful recipes we refer to Stanimirović (2002). The application of such a correction is not an easy job, but taking various caveats into account, all of the methods can produce comparable results. It is important to note that the CGPS, SGPS, and VGPS surveys have been corrected for the missing short-spacing data. The data quality is excellent, as shown by Stil et al. (2006b) who made a few data checks and intercomparisons.

**2.2.4. Field-programmable-gate-array spectrometer.** With the advent of field-programmable-gate-arrays (FPGAs) and fast analog-digital converters (ADCs), new radio astronomical spectrometers became accessible within the past few years. FPGA spectrometers combine large bandwidths (up to gigahertz), high dynamic ranges (8 to 14 bits), fast readout, high stability, and a high number of spectral channels with an affordable price (Mock 2004; Benz et al. 2005; Stanko, Klein & Kerp 2005). The technological leap in radio spectrometers was feasible; because the ADC sampling rate increased up to 4 GHz, further progress is expected. Considering that the transformation of a temporal continuous but band-pass-limited signal by an ADC produces a series of discrete spectra, this provides the possibility of digital undersampling (or Super-Nyquist sampling). Using a bandpass filter in front of the ADC allows us to select the Nyquist band of interest. Because of the digital undersampling, the Nyquist band of interest is detectable in the baseband (ranging from 0 Hz to the bandwidth limit).

Because of the rapid technological development of ADCs and the “programmable hardware” of FPGAs, FPGA spectrometry has the potential to replace, in the near future, auto-correlators and filter-band spectrometers entirely. They are the key for future instrumentation with respect to the increasing demand on bandwidth, spectral channels, and number of feeds. The ADC determines the bandwidth and the dynamic range, while the number of logical elements implemented within the FPGA determines the number of spectral channels. Using Fast-Fourier Transformation or Poly-phased Filter codes written in Very High Speed Integrated Circuit Hardware Description

Language, it is feasible to realize data storage times (dump times) of less than a second, which is very favorable for RFI mitigation strategies.

**2.2.5. Radio frequency interference mitigation.** RFI causes severe limitations on the sensitivity of radio telescopes in general. Even within the protected H<sub>I</sub> 21-cm line, band irradiation of RFI signals is common. The sources of the RFI are as manyfold as the number of electronic devices used today. In particular, digitally operating devices pollute a broad frequency range because of their extremely sharp defined band-passes. These sharp “frequency edges” produce high harmonics at different power levels that degrade the observational data. Also, aging of electronic components may alter the performance of the electronic circuits, thus causing RFI. Moreover, the pollution of the astronomical signals by RFI is getting more serious because of the increasing sensitivity of radio astronomical receivers and the scientific interest in even fainter emission lines. RFI is received not only by the main antenna beam but also by the side lobes and even from the backside of the dish. Strong RFI signals are orders of magnitude more intense than the radio astronomical signal of interest. Because of the limited dynamic range of auto-correlators, strong RFI signals may saturate them. The high dynamic range of FPGA-spectrometry allows us to overcome this limitation. The faint RFI signals are, however, the most problematic ones. They cannot be identified within a single spectrum and may change their intensity, frequency, and polarization properties on timescales shorter than the integration time. This leads to a degradation of the H<sub>I</sub> spectrum, which is extremely difficult to identify (Winkel et al. 2007).

With respect to 21-cm emission lines, high temporal resolution is an extremely valuable property of FPGA-spectrometers because it allows us to distinguish between astronomical and RFI signals. Most of the RFI signals can be identified by frequency variations, intensity modulations, and changes of their polarization properties. The variability of these properties clearly distinguishes RFI signals from the H<sub>I</sub> 21-cm line emission of astronomical sources. Using high-speed personal computers, it is feasible to perform an off-line search for temporal variable signals within the H<sub>I</sub> spectra to mitigate the degradation of the astronomical data by man-made radio noise.

For a recent overview of different RFI mitigation strategies see, e.g., Ekers & Bell (2001), Winkel et al. (2007), and Fridman (2008).

## 3. H<sub>I</sub> ON THE GALACTIC SCALE

### 3.1. The Disk

Observations of spiral galaxies teach us, in general that many H<sub>I</sub> disks have typically three times the extent of their stellar distribution. According to this, H<sub>I</sub> is considered to be an extremely sensitive tracer of the Galactic mass distribution and of the dynamics of Galactic systems as a whole. We intend to discuss first global aspects of the H<sub>I</sub> distribution in the Milky Way, in particular the vertical and radial extension of the H<sub>I</sub> disk. We use Galactocentric cylindrical coordinates  $R$ ,  $z$ , and  $\phi$ ; the Sun is at azimuth  $\phi = 180^\circ$ .

**3.1.1. Rotation curve.** Brightness temperatures  $T_B(l, b, \nu)$  observed in Galactic coordinates with longitude  $l$  and latitude  $b$  need to be converted into volume densities  $n(R, z)$  (Burton & te Lintel Hekkert 1986, Diplás & Savage 1991). Assuming that most of the gas follows an axisymmetric circular rotation yields the well-known relation for the differential rotation velocity (e.g., Burton 1988)

$$v(R, z) = \left[ \frac{R_\odot}{R} \Theta(R, z) - \Theta_\odot \right] \sin l \cdot \cos b. \quad (1)$$

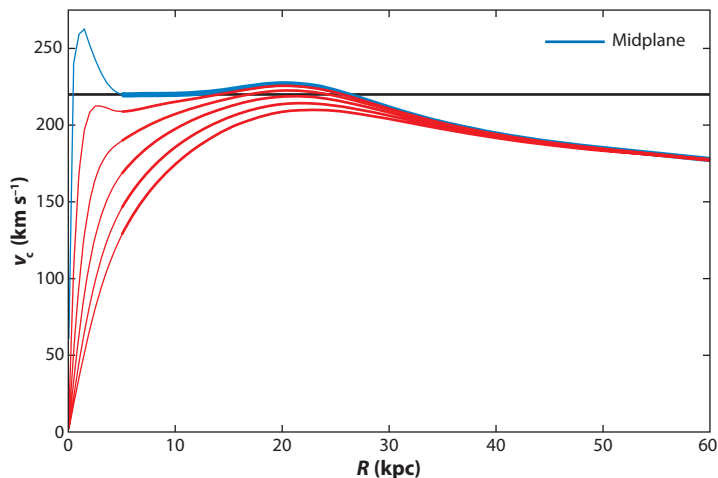


**Figure 2**

Mean axisymmetric Milky Way rotation curve according to Kalberla et al. (2007). The upper blue curve represents the rotation curve at midplane. The case  $v = 220 \text{ km s}^{-1}$  is plotted for comparison. The curves below (*red*) show the circular streaming velocities for gas layers offset from midplane at the position of the Sun by  $|z| = 1$  to 5 kpc. The lags are caused by gravitational effects only. Noncircular motions affect rotation velocities significantly for  $R < 5 \text{ kpc}$  (*thin lines*); these data are not used.

$v$  denotes the radial velocity along the line of sight, while  $\Theta(z)$  denotes the tangential velocity at a certain radius  $R$ . In the inner Galaxy, for  $R < R_\odot$ , distances are ambiguous, except for terminal velocities. To solve this equation for  $R > R_\odot$ , one needs to know the Galactic constants  $R_\odot$  and  $\Theta_\odot$ , but also the rotation curve  $\Theta(R, z)$ . Here we use  $R_\odot = 8.5 \text{ kpc}$  and  $\Theta_\odot = 220 \text{ km s}^{-1}$ . A further uncertainty is caused by noncircular motions owing to the central bar (Burton & Liszt 1993). The rotation is also poorly known in the outer Galaxy because it is particularly difficult to determine accurate distances there. Systematic biases can seriously degrade the derivation of the rotation curve (Binney & Dehnen 1997). Within the past decade a general consensus on the flatness of the outer rotation curve is accepted [e.g., Fich, Blitz & Stark (1989) and applications by Levine, Blitz & Heiles (2006a,b)]. Attempts to solve the combined Poisson-Boltzmann equation to describe the HI flaring in a self-consistent way result in a rotation curve that is approximately flat within  $5 \lesssim R \lesssim 27 \text{ kpc}$  (Kalberla et al. 2007). In the following, we use this rotation curve shown in **Figure 2**. This yields results that are compatible with those derived previously for a flat rotation curve. Major differences, however, may be caused by the fact that we abandon a cylindrical rotation law. At distances  $|z| > 0$  we use a lagging rotation (for details see Section 3.2.5).

The derivation of such a rotation depends inherently on the baryonic and nonbaryonic matter distribution of the Milky Way Galaxy. A Galactic mass model can be formulated in a self-consistent fashion if one drops the assumption of a dark matter (DM)-free Galactic disk (Kuijken & Gilmore 1989). The best fit mass model can be characterized by a thick self-gravitating DM disk with  $M = 1.8 \times 10^{11} M_\odot$  and a ring-like component with  $M \sim 2.3 \times 10^{10} M_\odot$  located at  $13 < R < 18.5 \text{ kpc}$ . It remains an open question whether such a DM distribution can result from accretion events (Read et al. 2008). For the Kalberla et al. (2007) model the total mass within  $R \lesssim 60 \text{ kpc}$  is  $M = 4.6 \times 10^{11} M_\odot$ . Baryons provide  $M = 9.5 \times 10^{10} M_\odot$  with a gas fraction of 13%. The HI mass is  $M = 8 \times 10^9 M_\odot$ , the warm ionized medium contributes  $M = 2 \times 10^9 M_\odot$ , and molecular gas is  $M = 2.5 \times 10^9 M_\odot$ .

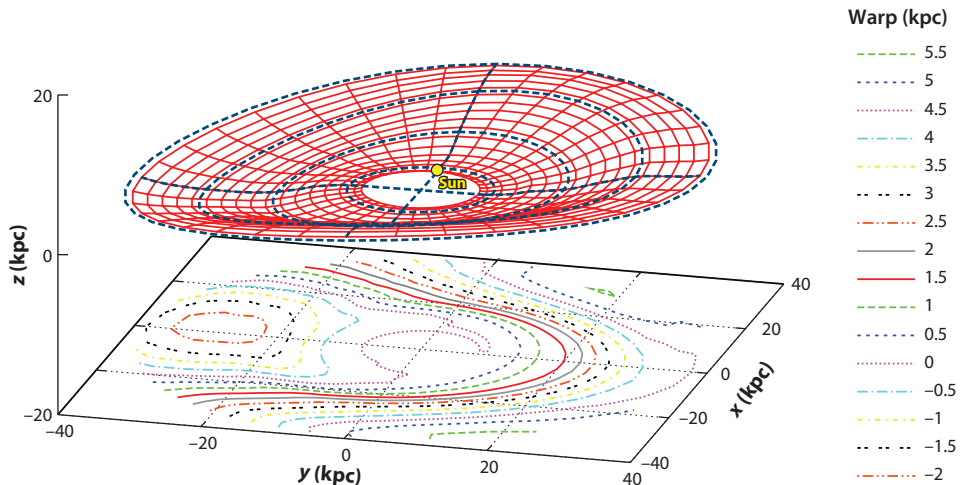


**Figure 3**

The warped Galactic plane; average midplane positions as derived from the Leiden-Argentine-Bonn 21-cm line survey by fitting three basic modes. Isophotes are from  $z_0 = -2$  to 5.5 kpc in steps of 0.5 kpc. The  $z = 0$  plane is inclined by  $60^\circ$  and viewed from  $\phi = 15^\circ$ . The location of the Sun is indicated by the yellow dot. The blue dashed lines mark quadrants in azimuth and distances  $R = 10, 20, 30,$  and  $40$  kpc, respectively.

Unfortunately, the straightforward solution of Equation 1 yields large north/south asymmetries in the column density distribution of the outer disk, which leads to vital debates on their origins (e.g., Kerr 1962, Blitz & Spergel 1991, Kuijken & Tremaine 1994). Levine, Blitz & Heiles (2006a) solved the asymmetries by assuming elliptical gas orbits. Large-scale mass asymmetries are found to be consistent with this empirical approach (Kalberla et al. 2007); deviations can amount to  $\sim 15 \text{ km s}^{-1}$  at  $R \sim 25$  kpc.

**3.1.2. The warp.** For a description of the global properties of the HI distribution in the Milky Way it is necessary to consider the bending of the Galactic plane (Henderson, Jackson & Kerr 1982), noticeable at  $R \gtrsim 9$  kpc in HI but also in CO clouds, in stars, in HII regions, and in other tracers (Wouterloot et al. 1990). The reliability of the LAB database makes it possible to extend the determination of the HI warp parameters out to large Galactocentric radii, where the HI emission lines show up as faint profile wings at large velocities. Levine, Blitz & Heiles (2006a) identified three basic warp modes for  $R \lesssim 30$  kpc. Kalberla et al. (2007) extended their analyses and found that these warp modes remain surprisingly well defined even out to  $R \sim 40$  kpc. **Figure 3** displays a perspective view of the warped plane  $z_0(R, \phi)$  looking approximately across the center in a direction toward the Sun.

**3.1.3. Midplane and surface density distribution.** Taking the warp into account it is possible to derive the average HI volume density  $n_0(R)$  at midplane (**Figure 4**). The radial distribution is approximately exponential for  $7 \lesssim R \lesssim 35$  kpc;  $n(R, z_0) \sim n_0 \cdot e^{-(R-R_\odot)/R_n}$  with  $n_0 = 0.9 \text{ cm}^{-3}$  and  $R_n = 3.15$  kpc. There are systematic differences between the northern and southern parts of the disk in the azimuth ranges of  $0^\circ < \phi < 180^\circ$  and  $180^\circ < \phi < 360^\circ$ , which has been known for a long time (e.g., Kerr 1962). For radii in excess of  $R = 15$  kpc, the dominant fraction of the neutral gas is located in the Southern Hemisphere. A similar trend  $n(R) \approx e^{-0.3R}$  was found by Strasser & Taylor (2004) from CGPS data with  $R \lesssim 20$  kpc.

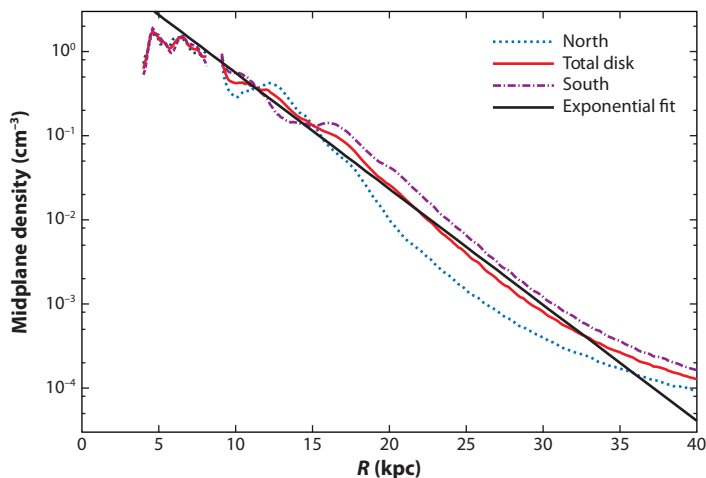


**Figure 4**

Average midplane volume densities as a function of  $R$ . The red line marks the total average, the dotted blue line the northern, and the purple dashed line the southern part separately. The black line shows the exponential fit with a scale length  $R_n = 3.15$  kpc (from Kalberla & Dedes 2008).

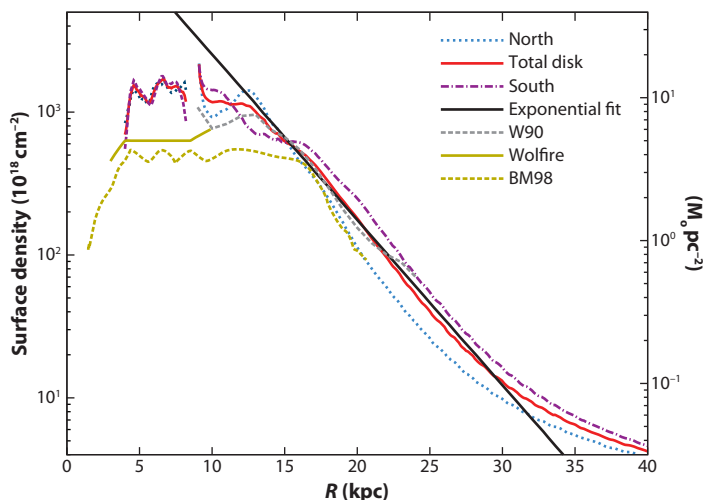


**Figure 5**

Average surface density distribution as a function of  $R$ . The red line marks the total average, the dotted blue line the northern, and the purple dashed line the southern part separately. The black line shows the exponential fit with a scale length  $R_s = 3.75$  kpc (Kalberla & Dedes 2008). The dotted gray line reproduces the distribution published by Wouterloot et al. (1990, W90), the thick yellow line reproduces data used by Wolfire et al. (2003), and the dashed yellow line reproduces the distribution published by Binney & Merrifield (1998, figure 9.19, BM98).

The average surface density distribution is plotted in **Figure 5** and can be approximated by  $\Sigma(R) \sim s_0 \cdot e^{-(R-R_\odot)/R_s}$  with  $s_0 = 30 M_\odot \text{ pc}^{-2}$  and  $R_s = 3.75$  kpc. There are similar systematic differences between the northern and southern sky as there are for the midplane densities (see **Figure 4**). For large radial distances the derived distribution is in good agreement with previous investigations (e.g., Wouterloot et al. 1990, Diplas & Savage 1991), but there are some degradations

for  $R \lesssim 12.5$  kpc. The surface densities saturate at approximately  $\Sigma_{inner} \sim 10M_{\odot} \text{ pc}^{-2}$ . To overcome this limitation, it is common to use the value  $\Sigma = 5M_{\odot} \text{ pc}^{-2}$  (Dickey & Lockman 1990). The average surface densities according to Binney & Merrifield (1998, figure 9.19) are even lower but may be affected by a systematic bias (Lockman 2002a). Wolfire et al. (2003) used a slightly larger estimate with a local maximum at  $R \sim 13$  kpc. For comparison, we show these surface densities in **Figure 5**.

**3.1.4. HI scale height.** The average scale height  $b_z(R)$  of the HI disk depends on the balance between gravitational forces and the pressure constituents. Analogous to planetary atmospheres, one may approximate this situation as a “Galactic atmosphere” by a hydrostatic equilibrium approach. This, however, implies a very global approach because on scales up to at least hundreds of parsecs the pressure and density of the ISM may be highly variable and far from equilibrium. Dynamical aspects, turbulence, and phase transitions are discussed later. Here we assume that the global HI distribution in the Milky Way disk can be considered on these large scales as in a steady state. The average thickness  $b_z(R)$  (half width at half maximum, HWHM) of the HI disk shows a pronounced flaring (**Figure 6**) that can be approximated by an exponential relation  $b_R = b_0 e^{(R-R_0)/R_0}$  kpc with  $b_0 = 0.15$  kpc and  $R_0 = 9.8$  kpc for  $5 \lesssim R \lesssim 35$  kpc.

Flaring may be induced by changes of the gravitational potential in the  $z$  direction or by variations in the heating/cooling balance of the HI gas. Observing the HI gas in our own Galaxy has the advantage that we are able to resolve the emission lines of individual regions. The situation in our own Galaxy is luckily very different from that in external systems, because only for our Galaxy do we really know the viewing inclination and the position of the line of nodes. For external systems, the observational data are highly distorted, implying that the Milky Way is the prime example for such an analysis. There are no indications that turbulence or multiphase properties of the HI gas depend significantly on radial distance  $R$ . The flaring may therefore be used to probe DM models (e.g., Narayan, Saha & Jog 2005; Sánchez-Salcedo, Saha & Narayan 2008). A

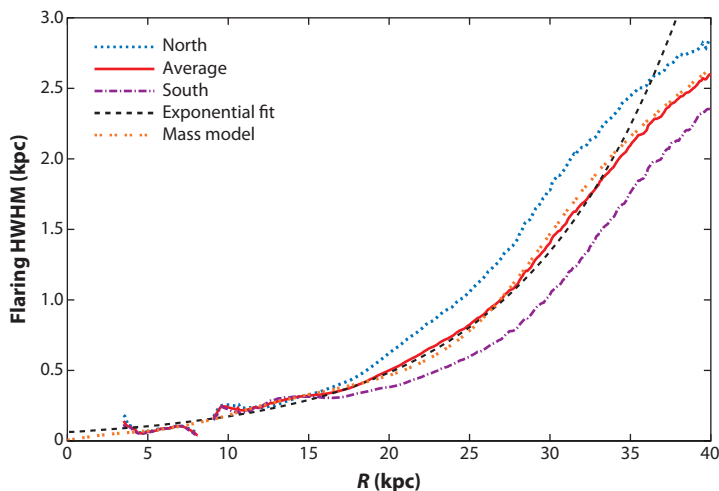


**Figure 6**

Average flaring of the HI gas layer as a function of  $R$  (from Kalberla & Dedes 2008). The observations can be approximated very well by an exponential relation (*black dashed line*) or by fitting a mass model to an isothermal HI gas distribution (Kalberla et al. 2007).

self-consistent solution of the Poisson-Boltzmann equation implies a disk-like DM distribution and a flat rotation curve (Kalberla et al. 2007).

**3.1.5. The exponential disk.** Figures 4 through 6 show that within the uncertainties the global properties of the HI gas in the disk can be well approximated by exponential distributions. A correlation between these parameters is expected because on average the surface density, the midplane density, and the scale height are related according to  $\langle \Sigma(R) \rangle \approx \langle n_0(R) \rangle \cdot \langle b_z(R) \rangle$ . In the outer part of the Milky Way disk, this approximation remains valid up to  $R \sim 35$  kpc, this radius apparently defines the outer edge of the Galactic disk. From the mass model this distance distinguishes the transition from the inner oblate gravitational potential to a prolate one. Clearly the disk approximation breaks down at this radius. This limit is approximately three times the radius  $R_{25}$  of the stellar disk. For spiral galaxies such a ratio is frequently observed; we conclude that the Milky Way may be quite normal in this respect.

**3.1.6. Optical depth effects.** A closer look to the exponential relations, comparing the scale lengths in detail, shows a small but significant deviation from the exponential disk approximation. Our discussion of the global distributions  $\Sigma(R)$ ,  $n_0(R)$ , and  $b_z(R)$  assumed that the HI gas is optically thin.

Optical depth effects have been discussed by Burton (1976). The more recent CGPS data show that optical depth biases increase with increasing observed column density (Strasser & Taylor 2004); for Strasser & Taylor's sample the emission traces only 75% of the HI gas. A similar result for the SGPS was given by Dickey et al. (2003). Kolpak et al. (2002) derive a general trend of increasing optical depth with decreasing  $R$  as well as a strong correlation with the molecular gas content. Unfortunately, their analysis is restricted to low Galactic latitudes only,  $b \lesssim 0^\circ.7$ . All these investigations show common trends and serious biases for  $R \lesssim 12$  kpc (see Figure 5), but are unfortunately insufficient for a statistical correction of optical depth as a function of  $R$ .

**3.1.7. Spiral structure.** The driver for early investigations of the HI distribution in the Milky Way was a quest to determine the spiral structure but the data were largely over interpreted. Aiming to derive a more detailed picture from actual HI survey data leads to frustrating results. Large-scale maps of the HI surface density distribution do not give clear evidence for a spiral structure. Major problems are distortions due to turbulent streaming motions along the line of sight that are confusing the velocity-distance transformation. Also, flow patterns revealing an arm are governed by the nonlinear density wave theory, so that the HI does not appear at the mass locus of the arm. However, some spiral structure may be disclosed as perturbations in the surface density distribution. Levine, Blitz & Heiles (2006b), using surface densities for  $R < 25$  kpc from the LAB survey, derived parameters for four nonaxisymmetric logarithmic spirals with pitch angles of  $20^\circ$  to  $25^\circ$ . They have shown also that overdensities in the surface density distribution are coincident with regions of a reduced thickness of the gas layer. Each of the arms has already been detected previously, including the prominent one in the fourth quadrant, which was studied in detail by McClure-Griffiths et al. (2004). SGPS data disclose an extension over  $70^\circ$ ; over most of its length, the arm is 1–2 kpc thick.

A systematic depression in the scale height of the gas may be interpreted as an indication for associated enhancements in the mass distribution. Kalberla et al. (2007) compared observed HI scale heights with average scale heights from an axisymmetric mass model. They could trace the spiral arms suggested by Levine, Blitz & Heiles (2006b) up  $R \sim 30$  kpc; for the best defined arm they could trace it even up to  $R \sim 35$  kpc. The mass model implies that spiral arms trace mass enhancements by a factor of 3 to 6 with respect to the average axisymmetric density.

---

**IVC:** intermediate-velocity cloud

---

### 3.2. The Disk-Halo Interface

Pictures of the H I distribution show numerous filaments extending to high Galactic latitudes (e.g., Hartmann & Burton 1997). Individual clouds and coherent cloud assemblies (or complexes) can be easily distinguished from the Galactic disk emission because of their deviation velocities (Wakker 1991). They are denoted as intermediate- and high-velocity clouds, respectively (IVCs and HVCs); excellent reviews are available from Wakker & van Woerden (1997) and the collection of chapters in the book edited by van Woerden et al. (2004).

In addition to these two populations of halo clouds there have long been indications for a third population, an “envelope of H I surrounding the spiral structure” (Shane 1967), reported for the first time by Oort (1962). First observations date back to Prata (1964) and Simonson (1971); such clouds are obvious in the LDS data.

**3.2.1. Halo clumps.** Lockman (2002b) was the first to study this population at high resolution. Using the GBT, he searched the first Galactic quadrant and used the terminal velocity method to determine distances of individual clouds. In many cases the clumps are embedded in faint diffuse filaments that are connected to the disk. Other clumps appear to be spatially associated with the disk, but their velocities are high and unexpected. The clouds are found at  $z$  distances up to 1.5 kpc. Clouds that reach high  $z$  distances need large vertical velocities to overcome the gravitational attraction of the Galactic disk. In the median, the clouds have diameters of  $\sim 20$  pc, peak column densities of a few times  $10^{19}$   $\text{cm}^{-2}$ , H I densities of a few tens  $\text{cm}^{-3}$ , and H I masses of  $50 M_{\odot}$ . Some of the lines are narrow, indicating gas at temperatures of less than 1000 K. The spectra also show evidence for a core-halo velocity structure. Lockman (2002b) concluded that as much as half the mass of the neutral halo could be contained in clouds.

In the meantime, Stil et al. (2006a) identified fast moving clumps within the plane of the Galactic disk. The current interpretation is that both ensembles of clouds belong to the same population. Ongoing searches with the Parkes telescope in the fourth quadrant by Ford et al. (2008), with Arecibo (Stanimirović et al. 2006), and the Effelsberg telescope (Dedes 2008) in regions even beyond the Solar circle indicate that this population is probably widespread throughout the whole Milky Way. The approximate average detection rate for these telescopes is one cloud per two square degrees. The apparent distribution of this cloud ensemble in Galactic coordinates, hence the detectability, is influenced by projection effects (Kalberla & Dedes 2008).

The LAB survey does not allow us to resolve the individual clumps, but provides statistical evidence that about 10% of the H I gas is located outside the disk. **Figure 7** shows the average H I emission in the direction toward both Galactic poles for latitudes  $|b| > 20^{\circ}$ . We use a logarithmic brightness temperature scale to display the huge dynamic range in  $T_{\text{B}}$ . The peak emission close to  $v_{\text{LSR}} = 0$   $\text{km s}^{-1}$  is associated with faint but extremely broad wings. In the south, for  $b < -20^{\circ}$  (*blue* in **Figure 7**), the wing at positive velocities is dominated by emission from the Magellanic stream. IVCs lead to enhanced emission at  $v_{\text{LSR}} \sim -50$   $\text{km s}^{-1}$ , but elsewhere one observes a remarkable symmetric distribution for both negative and positive velocities. These wings, first published by Stark et al. (1992, their figure 10), are highly suggestive of stray radiation but it can be shown that they are real (Verschuur 2004, Haud & Kalberla 2006, Kalberla & Dedes 2008). Adopting the interpretation that the local neutral ISM is supported in the Galactic gravitational potential primarily by turbulence (Dickey & Lockman 1990, Lockman & Gehman 1991) implies high random velocities for individual clouds.

The H I spectra can be fitted by a population of unresolved clouds with a velocity dispersion of  $\sigma \sim 74$   $\text{km s}^{-1}$  (Kalberla & Dedes 2008). This is more than a factor of three larger than the typical velocity dispersion of H I gas, implying that this gas component exceeds the kinetic energy

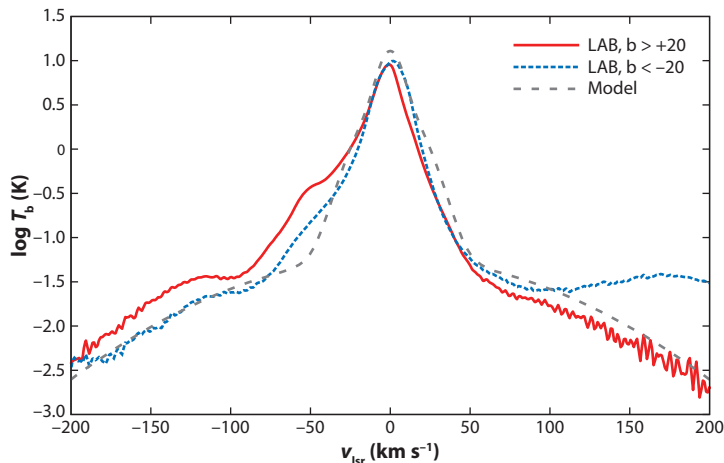


**Figure 7**

Average 21-cm HI line emission for latitudes  $|b| > 20^\circ$  from the LAB survey as a function of radial velocity  $v_{\text{lsr}}$ . The red line marks the north polar cap and the dotted blue line the southern part. The dashed black line represents the model (Kalberla & Dedes 2008).

of the disk gas by an order of magnitude. Such fast clouds can reach  $z$  distances of 4 kpc near the Sun. Including flaring in our considerations, this is consistent with heights observed by Lockman (2002b) and Ford et al. (2008) for the HI clumps in the inner part of the Milky Way.

**3.2.2. The halo.** The definition of the halo is quite a problem. We have a smooth transition of temperature, volume density, and pressure with increasing altitude. Assuming a hydrostatic equilibrium approximation on a Galactic scale, we can deduce from the LAB survey a vertical scale height at the location of the Sun for the CNM of 150 pc, for the WNM of 400 pc, and for a very faint halo gas component of 4 kpc (see Kalberla 2003, his table 1). The corresponding midplane volume densities (for CNM,  $0.3 \text{ cm}^{-3}$ ; WNM,  $0.1 \text{ cm}^{-3}$ ; and halo gas,  $0.001 \text{ cm}^{-3}$ ) decrease roughly linearly proportional to the vertical scale height of the gas component. There are ionized as well as neutral gas structures at kiloparsec distances from the Galactic plane; the Milky Way Galaxy is enclosed within a gaseous “atmosphere”. Tidal gas streams as well as “classical” HVCs and complexes at distances of tens of kiloparsecs may be embedded within this atmosphere. Considering the radial velocities of the HVC complexes, a few  $100 \text{ km s}^{-1}$ , moderate to strong shocks are expected to be observed in the disk-halo interface. HVCs are prominent because they are part of large and massive complexes that are forming coherent structures.

Observational evidence for an extended gaseous halo is also given by the fact that most of the HVC complexes show a pronounced multiphase structure (Kalberla & Haud 2006). Gas pressure from the confining gaseous halo supports phase transitions (Wolfire et al. 1995b). HVCs have turbulent energy densities that are an order of magnitude larger than that of comparable clumps in the Galactic disk.

**3.2.3. Asymmetries.** The average HI distribution has significant north-south asymmetries, obvious since the very first HI observations. The differences are most pronounced for  $20 \lesssim R \lesssim 30 \text{ kpc}$ . The HI scale heights are lower in the south, implying local enhancements in the gravitational potential caused by asymmetries in the DM distribution. As a response, the circular velocities are

estimated to increase up to  $15 \text{ km s}^{-1}$  (Kalberla et al. 2007), consistent with the empirical epicyclic streamline correction by Levine, Blitz & Heiles (2006a).

**3.2.4. The outskirts.** Toward the outskirts of the Milky Way, for  $R \gtrsim 35 \text{ kpc}$ , the average HI distribution does not fade off exponentially. **Figures 4** and **5** imply for  $R \gtrsim 35 \text{ kpc}$  a faint distribution of HI gas that encloses the exponential HI disk. We display in **Figure 8** a more detailed comparison. Surface densities, calculated for several azimuthal sectors with  $-15 < z < 20 \text{ kpc}$  deviate for  $R \gtrsim 35 \text{ kpc}$  significantly from the exponential disk distribution. Asymmetries are less pronounced than for  $R \lesssim 35 \text{ kpc}$  (Section 3.1.3, **Figures 4** and **5**).

The parameters of the highly turbulent HI phase, which were found to fit the extended profile wings observed toward the polar caps, have also been used to model HI emission for all distances  $R < 60 \text{ kpc}$ . A radial exponential scale length of  $R_h = 7.5 \text{ kpc}$  (Kalberla 2003), twice the disk scale length  $R_s$ , discussed in Section 3.1.3, was used. The resulting component is plotted with a red line and compares well with the observational data. It is remarkable that parameters that were derived to explain local emission features in the direction to the poles (Section 3.2.1) are useful also at  $R > 35 \text{ kpc}$ .

Comparing this finding with the distribution of the anomalous gas phase in a few other galaxies (e.g., Fraternali 2008, Fraternali & Binney 2008), it would be consistent if the Milky Way CNM and WNM disks are also surrounded by a patchy and highly turbulent halo medium. About 10% of the total HI gas may be in this phase (Kalberla & Dedes 2008).

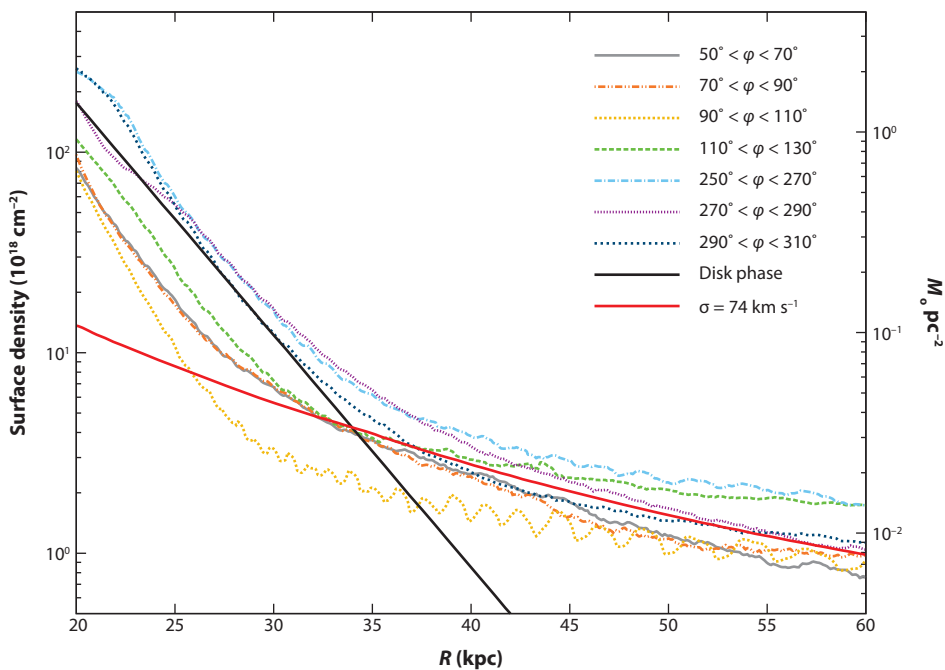


**Figure 8**

Average surface densities as a function of  $R$  for  $20^\circ$ -wide radial sectors in the outskirts of the Milky Way. For comparison, the fitted distribution for the disk gas (*solid black line*) as well as for a turbulent halo medium with  $\sigma \sim 74 \text{ km s}^{-1}$  (*solid red line*) is given (Kalberla & Dedes 2008).

**3.2.5. The corotation problem.** For a steady-state gas in an axisymmetric gravitational potential, the average azimuthal streaming velocity  $\bar{v}_\phi(z)$  can be derived from Euler's equation

$$(\bar{v} \cdot \nabla)\bar{v} = -\frac{\nabla p}{\rho} - \nabla\Phi, \quad (2)$$

where  $\rho$  is the volume density and  $p$  is the pressure of the gas; in the isothermal case  $p \propto \rho\sigma^2$ .  $\Phi$  denotes the gravitational potential and  $\bar{v}$  the velocity vector. Equation 2 excludes magnetic and viscosity terms. For an ideal gas with an isotropic velocity dispersion, which can be described by a barotropic equation of state  $p = f(\rho)$ , York et al. (1982) have shown that the extraplanar gas must be corotating with the disk.

A multiphase medium violates the barotropic condition, a fact that is often disregarded; corotation may therefore not be taken for granted. To quantify how far rotation is affected by the gravitational potential  $\Phi$ , we set  $\nabla p/\rho = 0$ . With increasing  $|z|$  distance, the gravitational forces acting on the gas decrease, implying a lower average streaming velocity. The expected velocity deviation  $\Delta v(R, z) = \bar{v}_\phi(R, z) - \bar{v}_\phi(R, 0)$  depends on the mass model; at constant  $z$  distances  $\Delta v(R, z)$  depends strongly on  $R$  (**Figure 2**). Fortunately, the situation is simplified considerably if the gravitational forces within a Galactic disk are dominated by a massive exponential disk. In this case, the vertical gradient in the rotation speed  $\Delta v(R, z_b)$  is approximately constant for constant normalized distances  $z_b(R) = z(R)/b_z(R)$  (Kalberla 2003). Flaring gas layers share a similar lag if we evaluate  $z$  distances of the layers normalized to scale height  $b_z(R)$ .

In **Figure 9** we estimate  $\Delta v(R, z_b)$  for a Milky Way mass distribution as advocated by Kalberla et al. (2007). For CNM/WNM gas located one exponential scale height above midplane, we get  $\Delta v \gtrsim -1.3 \text{ km s}^{-1}/\text{scale height}$  (*red line*). Previously, HI observations were interpreted such that in the inner part of the Milky Way corotation is present up to a  $z$  distance of 1 kpc (e.g., Dickey & Lockman 1990). Recent analyses of the VGPS and SGPS by Levine, Heiles & Blitz (2008) show a radically different picture. For  $3 < R < 8 \text{ kpc}$ , the vertical falloff in the rotation curve within

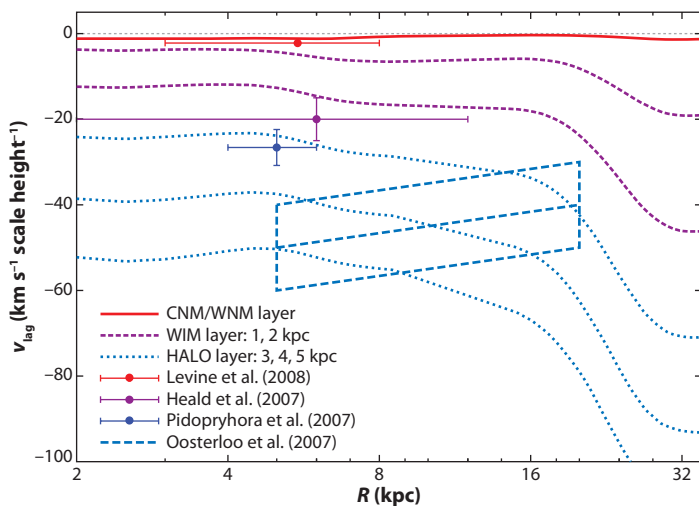


**Figure 9**

Vertical gradient in rotation velocity normalized to the vertical scale height. Red, gradient expected for the Milky Way HI layer consisting of CNM/WNM gas compared with results by Levine, Heiles & Blitz (2008). Purple, gradient for the warm ionized medium at a local scale height of 1 and 2 kpc and observational results by Heald et al. (2007) from external galaxies. Blue, gradient for the halo layer at a local scale height of 3 to 4 kpc. The data are derived from Pidopryhora et al. (2007) and Oosterloo, Fraternali & Sancisi (2007).

---

**WIM:** warm ionized medium

---

100 pc of the Galactic midplane is after all  $-22 \pm 6 \text{ km s}^{-1} \text{ kpc}^{-1}$ . For  $b_z(R) \sim 100 \text{ pc}$ , this gives  $\Delta v \sim 2.2 \text{ km s}^{-1}/\text{scale height}$ , a noticeable lag and within the uncertainties consistent with the model.

**Figure 9** includes estimates of  $\Delta v(R, z_b)$  for the warm ionized medium (WIM) with scale heights of 1 or 2 kpc (*purple*). Measurements within the Milky Way are missing but Heald et al. (2007) derived  $\Delta v = 15$  to  $25 \text{ km s}^{-1}/\text{scale height}$  for the extraplanar diffuse ionized gas (EDIG) emission in three edge-on spiral galaxies. This value matches, within the uncertainties, the expectations for a WIM scale height of  $b_z(R_\odot) \sim 2 \text{ kpc}$ , close to the most recent determination of  $b_z(R_\odot) = 1830^{+120}_{-250} \text{ pc}$  by Gaensler et al. (2008).

Estimates for a lagging halo are included in **Figure 9** for  $b_z(R_\odot) = 3, 4,$  and  $5 \text{ kpc}$ , respectively (*blue*). We add, for comparison,  $\Delta v = 27 \text{ km s}^{-1}/\text{scale height}$  from Pidopryhora et al. (2007), assuming that the tip of the Ophiuchus superbubble with a distance of 3.4 kpc above the Galactic plane is located in the halo. The blue box in **Figure 9** represents an estimate of the lagging halo rotation in NGC 891 according to Oosterloo et al. (2007). These results are consistent with a local halo scale height of  $b_z \sim 4 \text{ kpc}$  for the halo H I.

Disregarding the lagging halo rotation may lead to serious biases in the derived volume density distribution for the disk-halo interface (Kalberla et al. 2007, their figures 10–13). The currently available data are within the uncertainties consistent with the assumption that the vertical gradient in rotation velocity per unit scale height is dominated by gradients in the gravitational field of the Galactic disk. Influences from pressure gradients, magnetic fields, and viscosity terms appear negligible, but it should be taken into account that the observational determination of  $\Delta v(R, z_b)$  is difficult because rotational velocities and scale heights need to be determined independently. Useful data became available only very recently, and further improvements are needed for a more sophisticated treatment of the lagging halo problem.

## 4. THE GALACTIC ECOSYSTEM

Up to now we considered mostly global properties of the Milky Way H I gas distribution, assuming a steady state with a hydrostatic equilibrium situation that depends predominantly on distance  $R$ . Such an equilibrium situation is characterized by the fact that the typical turbulent pressure of the gas is considerably larger than the thermal pressure, at the position of the Sun by about a factor of ten. Supernova explosions are predominantly responsible for the excess kinetic energy. Shock fronts trigger phase transitions of the gas phase and determine velocities and densities of individual cloud fragments. But the structure of the ISM affects also the evolution of the supernova remnants. The interplay between supernovae and gas phase leads to feedback processes, eventually affecting the generation of giant molecular cloud complexes and subsequent star formation. Here we consider observational evidence for these highly dynamical processes.

### 4.1. Shells and Spurs

**Figure 10** shows the volume density distribution along the Galactic plane at a constant distance  $R = 15 \text{ kpc}$  from the Galactic center derived from the LAB survey. For comparison see figure 2 of Burton & te Lintel Hekkert (1986). Density concentrations at midplane and the Galactic warp are obvious. We used the first moment of the density distribution to define midplane and the second moment to determine the average dispersion of the gas in  $z$  direction; the white contours enclose the flaring disk at a  $3\text{-}\sigma$  level. This plot was derived from the LAB survey and includes H I gas at intermediate latitudes of  $-15^\circ < b < 20^\circ$ . It would be highly desirable to have a better spatial resolution for the derived density distribution, but numerous shells, spurs, and filaments are recognizable even at this moderate resolution. The plot shows that huge density contrasts

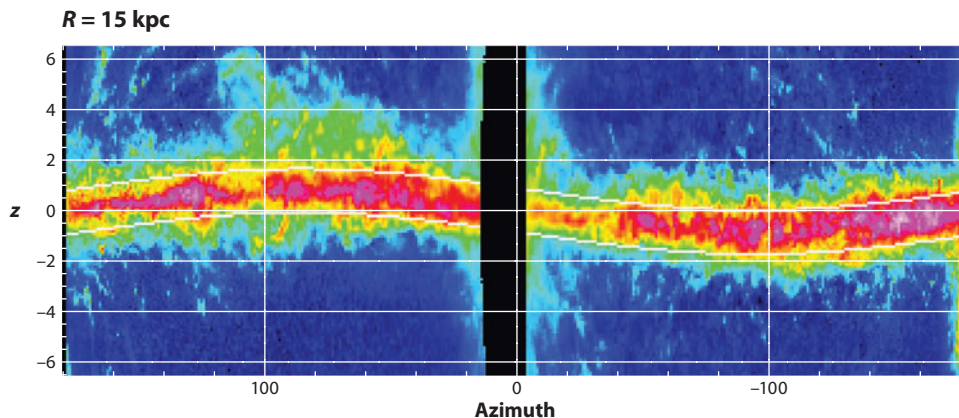


**Figure 10**

HI volume density distribution as a function of azimuth  $\phi$  and distance  $z$  for  $R = 15$  kpc. A logarithmic transfer function was chosen for  $n \lesssim 0.5 \text{ cm}^{-3}$  to enhance low-density regions. The white curves indicate the average scale height of the HI gas layer at a  $3\text{-}\sigma$  level and enclose the warped disk. Note that azimuth ranges of  $-30^\circ \lesssim \phi \lesssim 30^\circ$  are affected by the central bar; there are also ambiguities in the anticenter for  $150^\circ \lesssim \phi \lesssim 210^\circ$ .

can be associated with filaments. We have chosen a logarithmic transfer function to emphasize low-level emission reaching up to distances of  $z \sim 2$  kpc.

The derivation of **Figure 10** needs a sophisticated translation from observed brightness temperatures  $T_b(l, b, v)$  to densities  $n(R, z, \phi)$ , but HI shells are also observable in  $l, b, v$  data cubes. An initial search for HI shells in the northern sky was undertaken by Heiles (1979, 1984), and resulted in a compilation of 106 objects. Using LDS data for an automatic search, Ehlerová & Palouš (2005) found nearly 600 shell structures and derived statistical properties for 300 shells in the second quadrant. Searches toward the southern sky are missing so far, except for the range covered by the SGPS, where 19 new HI shells have been detected by McClure-Griffiths et al. (2002).

Search criteria for shells are usually that there needs to be a local minimum in the emission surrounded by a dense thin wall that is expanding and approximately spherical. Shells are found to be concentrated at midplane, 50% of them at  $|z| \lesssim 500$  pc and they appear to be preferentially located on the trailing edges of the spiral arms. The radial distribution can be approximated by an exponential law with a radial scale length of  $\sigma_{shell} = 3_{-1}^{+2}$  kpc (Ehlerová & Palouš 2005). This is somewhat larger than the scale length of the stellar disk, but note that it is easier to find shells in the outer Galaxy than in the inner. The size distribution follows a power-law  $dN(r_{sb}) = r_{sb}^{-\alpha} dr_{sb}$  with  $\alpha = 2.1 \pm 0.4$ . About 5% of the volume is occupied by shells. It is believed that shells are caused by supernovae and stellar winds that input  $10^{51}$ – $10^{53}$  ergs of energy into the ISM.

Supernovae in the Milky Way occur at a frequency of  $1.9 (\pm 1.1)$  events per century (Diehl et al. 2006). For a lifetime of  $\sim 10^6$  years, one expects  $\sim 2 \times 10^4$  remnants but far fewer are observed. Koo, Kang & Salter (2006) argue that the missing shells remain undetected because of selection criteria and suggest that faint velocity wings seen in 21-cm line surveys at high forbidden velocities could be indicative of these objects. These are the wings that were discussed in Section 3.2.1 as caused by a population of fast moving clouds. Koo, Kang & Salter (2006), searching for identifications of the wings, were able to prove in one case that the high-velocity wing was due to gas blown off from the disk by a supernova. Subsequently, Kang & Koo (2007) studied 87 faint velocity wings and found coincidences with SNR in six additional cases, but for 85% of the sources no identification could be derived.

Daigle, Joncas & Parizeau (2007) used neuronal networks to search for dynamical signatures of expanding bubbles in the CGPS. They got 7100 detections with a radial distribution as expected for an exponential disk but concluded that at most 23% of these objects could be associated with stellar progenitors. It is obvious that the detection rate is greatly enhanced if high-resolution surveys can be used but turbulence in the ISM is strong enough to cause serious confusion.

## 4.2. Dynamical Equilibrium

Supernovae trigger violent interactions that locally throw the ISM out of balance. However, observations suggest that supernova events happen frequently enough to support, on scales of several kiloparsecs, a dynamical equilibrium. The question arises whether the Galactic ecosystem itself, considering all phases and the stellar component in interaction and in feedback, may be responsible for this kind of equilibrium.

High-resolution 3D hydrodynamical simulations of the gas in the Milky Way, accounting for the collective effects of supernovae on the structure of the ISM, have been performed for the first time by de Avillez (2000) and de Avillez & Berry (2001). The model considers explicitly the input of energy and mass by isolated and correlated supernovae in the disk. Once disrupted by the explosions, the disk never returns to its initial state. A dynamical equilibrium in the gas in close agreement with the observations is reached after 80 Myear. The stability of the disk and the disk-halo interface are directly related to the supernova rate. The model results in scale heights and volume filling factors for the individual phases of the ISM that are in good agreement with the observations. Filaments and spurs reaching  $z$  distances of several kiloparsecs do not contradict an equilibrium situation but are part of the ecosystem.

We plot in **Figure 11** the local volume filling factors from a fit of the interstellar medium by Kalberla & Dedes (2008), taking the average emission at both polar caps into account. The filling factors are derived for a medium that is assumed to be, on average, in turbulent pressure equilibrium. The distribution contains CNM and WNM, supplemented by a neutral halo medium

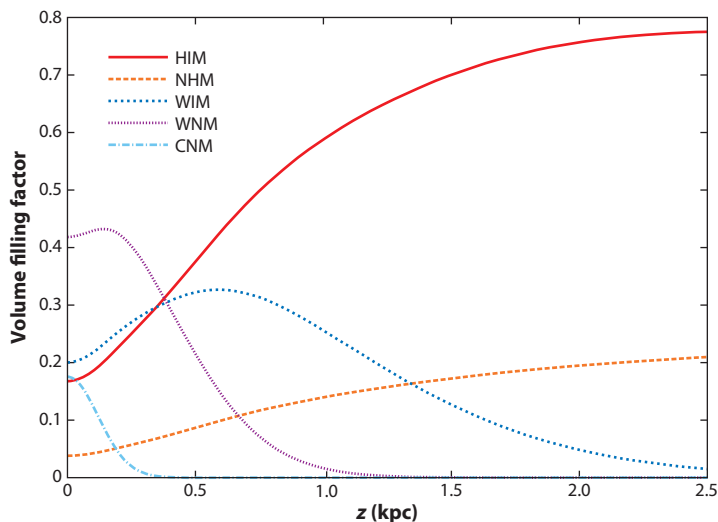


**Figure 11**

Volume filling factors for the local interstellar medium as a function of  $z$  distance derived from a hydrostatic model fit (Kalberla & Dedes 2008).

(NHM) embedded in the diffuse WIM and the hot  $10^6$  K plasma component (HIM) that dominates the halo at large  $z$  distances. **Figure 11** is in good agreement with figure 5 of de Avillez (2000) but leads to some adjustments of the first calculations by McKee & Ostriker (1977). Filling factors may vary; the hydrodynamical simulations show a time dependence and, in general, we need to assume that there is some additional (unknown) dependence on  $R$ .

---

**MM:** molecular medium

---

## 5. HI IN DIFFERENT PHASES

Neutral atomic hydrogen is an excellent tracer for the overall physical conditions within the Galactic ISM. Its abundance warrants that collisions are sufficiently frequent to populate the excited level.

From the observational point of view, the neutral gas traced by the H I 21-cm line comprises very different temperature and density regimes. Using the temperature as a measure for the physical state of the gaseous phase, we “classically” differentiate between the molecular medium (MM; around 10 K), the CNM (up to 100 K), the WNM (a few thousand K), the WIM ( $10^4$  K), and the HIM ( $10^6$  K). Also considering, the fact that a snapshot will reveal all these gaseous phases observable at the same time along many arbitrary lines of sight may suggest that there is some equilibrium arrangement. Pressure equilibrium appears essential, but we need to take into account that in addition to the well-known thermal gas pressure  $p_{\text{th}}$ , magnetic  $p_{\text{mag}}$  and cosmic-ray pressure  $p_{\text{cr}}$  contributions are significant. The turbulent pressure  $p_{\text{turb}}$  may even be dominating in most cases.

Each of these pressure components varies appreciably across the Milky Way disk and physical conditions of the gas may change considerably. Studying neutral atomic hydrogen means first focusing on the thermal pressure. If all the different gaseous phases are in equilibrium, the balance of the thermal pressure  $p_{\text{th}}/k \simeq nT$  [ $\text{K cm}^{-3}$ ] implies that the temperature  $T$  is inversely proportional to the volume density  $n$ .

### 5.1. Milky Way Gas within Different Environments

Focusing on the neutral hydrogen only, we have empirical evidence that, for column densities in excess of  $N_{\text{HI}} = 4 \cdot 10^{20} \text{ cm}^{-2}$ , the transition from atomic to MM may happen (Reach, Koo & Heiles 1994; Heithausen et al. 2001). Toward these denser H I clouds molecules of abundant species like  $^{12}\text{CO}$  and  $\text{NH}_3$  are observed. Molecular gas is also detectable toward much lower H I column densities (Richter, Sembach & Howk 2003), but not as a stable gas phase; it is most likely produced by temporal density and temperature fluctuations, far from equilibrium. As one of the general characteristics of the cold gas phase, we mention volume densities of  $n > 10^1 \text{ cm}^{-3}$ ,  $T < 100$  K, and a local exponential vertical scale height above the Galactic plane of  $b_z(R_\odot) \sim 150$  pc. Temperature and density are strongly coupled in equilibrium considerations via the thermal gas pressure, which is about  $2000 \text{ K cm}^{-3}$  in the case of the CNM.

Depending on the ionizing stellar radiation field and the environmental conditions within the plane, the CNM clouds are embedded within warm, ionized and perhaps coronal gas. Vertically the WNM is detectable across the whole sky with a 100% area filling factor. The WNM does not have a distinct internal cloud structure; it is diffuse and can be well approximated by a gas layer. The local scale height is  $b_z(R_\odot) \sim 400$  pc. The WIM shows in the Wisconsin H-Alpha Mapper survey (Haffner et al. 2003) some distinct sources, but these are also superposed on a diffuse background. In addition, dispersion measures from pulsar surveys clearly provide evidence for an “atmosphere” consisting of free electrons. The broadly used NE2001 model (<http://www.astro.cornell.edu/~cordes/NE2001/>) adopts a vertical scale height of about

1 kpc, but Gaensler et al. (2008) claim that this value is biased. Sight lines at low Galactic latitudes are contaminated by HII regions and spiral arms. Disregarding such data, they revise the WIM scale height to  $b_z(R_\odot) = 1830^{+120}_{-250}$  pc.

Finally, the HIM occupies the very neighborhood of active star-forming regions and a different phase fills the Galactic halo. Within the Galactic halo we find an associated neutral hydrogen gas phase at a low filling factor. This neutral hydrogen is in dynamical equilibrium with the hot gas but has to be considered as clumpy, a temporal phenomenon within the hot plasma (Pietz et al. 1998, Kalberla 2003).

## 5.2. Heating and Cooling, and Static Equilibrium

The classical differentiation of the gaseous phases relies on a physical background that is determined by the heating and cooling processes within the ISM. The relevant physical heating processes of the ISM are:

1. heating by low-energy cosmic rays (dense MM)
2. photoelectric heating by grains (CNM to MM)
3. photoelectric heating by photoionization of atoms and molecules (HII regions)
4. photoelectric heating by soft X-rays (WIM, WNM, CNM)
5. chemical heating (dense MM)
6. grain-gas thermal exchange (dense MM)
7. hydrodynamic and magnetohydrodynamic heating (WNM, CNM)
8. interstellar shocks (WNM, CNM, MM).

The list of heating processes compiled above indicates two important issues; first, the heating of the ISM is a function of position within the ISM and the properties of the ionizing source. Second, the efficiency of the heating depends on the physical and chemical conditions of the gas phase. Henceforward, we focus our discussion on the CNM and WNM, traced by the H I emission line.

The discussion of cooling of the neutral hydrogen gas is much briefer. Because of the low volume densities, we have to consider predominantly fine structure lines. These lines are observable in the far infrared regime, with the most important cooling line of singly ionized carbon at  $\lambda 157.7 \mu\text{m}$ . Owing to its low ionization potential below 13.6 eV and its high abundance, carbon dominates the cooling of neutral gas traced by the H I 21-cm line. Neutral oxygen is a coolant of less importance than carbon for the warm neutral gas because of its lower abundance. Its contribution is significant within the Galactic plane.

For the atomic phase of the neutral ISM an equilibrium equation between heating and cooling can be set up:

$$\Gamma_{\text{pe}} + \Gamma_{\text{X-ray}} = \Lambda_{\text{e,CII}} + \Lambda_{\text{H,CI}} + \Lambda_{\text{Ly}\alpha}. \quad (3)$$

Here  $\Gamma_{\text{pe}}$  denotes the photoelectric heating by dust grains,  $\Gamma_{\text{X-ray}}$  heating by soft X-rays,  $\Lambda_{\text{e,CII}}$  fine structure-line cooling by collisions between electrons and ionized carbon ions, and  $\Lambda_{\text{H,CI}}$  cooling by collisions between neutral hydrogen and neutral carbon atoms. Depending on the depletion factor of carbon on dust grains, the cooling efficiency is a function of environmental conditions.

In low volume density environments,  $n < 10^1 \text{ cm}^{-3}$ , typical for many CNM clouds, and the heating from the photoelectric effect on dust surfaces dominates over the X-ray heating by nearly an order of magnitude. Its absolute value ranges around  $\Gamma_{\text{pe}} \sim 2 \times 10^{-26} \text{ ergs s}^{-1} \text{ H}^{-1}$  and increases proportional to the volume density  $n$ . The heating by soft X-rays drops according to  $\sigma \propto E^{-\frac{3}{2}} \text{ cm}^3$  with increasing  $n$ .

At low volume densities,  $n < 1 \text{ cm}^{-3}$ ; like toward high Galactic altitudes, cooling by  $\text{Ly}\alpha$  photons and the corresponding metastable transitions is important  $\Lambda_{\text{Ly}\alpha}$ . In addition to this, the thin gas can be cooled by recombination of free electrons on dust surfaces. Both processes have nearly the same cooling efficiency,  $\Lambda \sim 7 \times 10^{-27} \text{ ergs s}^{-1} \text{ H}^{-1}$ . Above  $n = 1 \text{ cm}^{-3}$ , cooling by neutral oxygen and ionized carbon are of the same strengths and orders of magnitude more efficient than  $\text{Ly}\alpha$  or recombination of electrons onto the dust surfaces. The cooling power of ionized carbon increases with increasing  $n$ , while neutral oxygen drops rapidly with  $n$ . Neutral oxygen reaches a pronounced cooling peak around  $n = 1 \text{ cm}^{-3}$  with  $\Lambda_{\text{OI}} \sim 1 \times 10^{-26} \text{ ergs s}^{-1} \text{ H}^{-1}$  and drops by an order of magnitude for  $n \simeq 10 \text{ cm}^{-3}$ . Please note that all values are calculated assuming pressure equilibrium between all gaseous phases. According to this approach, density, pressure, and temperature are interrelated. The relevance of the different atomic species for cooling depends on the excitation potential (temperature) of the gas atoms.

Evaluating the different heating and cooling processes as a function of the volume density  $n$ , we find the characteristic tilted S-shape curve between pressure and volume density (**Figure 12**) (e.g., Wolfire et al. 1995a, their figures 4–7). This curve allows in low-pressure environments, for  $P/k \leq 1000 \text{ K cm}^{-3}$ , only a single warm (low volume density) gas phase. A single gaseous phase is also observable toward high pressure regions,  $P/k \geq 8000 \text{ K cm}^{-3}$ . In between, we find pressure equilibrium between warm and cold gas. Stable phases can exist only for  $dP/dn > 0$ , and this implies  $T \lesssim 300 \text{ K}$  for the CNM and  $T \gtrsim 5000 \text{ K}$  for the WNM. For  $dP/dn < 0$ , or at intermediate temperatures, the gas is considered to be unstable or transient. We denote this as the two-phase structure of the interstellar medium, which is considered to be typical for clouds up to distances of  $R \lesssim 18 \text{ kpc}$  from the Galactic center and a few tens of kiloparsecs above the disk (Wolfire et al. 1995a, 1995b, 2003). At larger radial distances the gas pressure decreases and one would expect that the CNM ceases. Surprisingly this is not observed. From CGPS, SGPS, and VGPS data it can be shown that the ratio of the emission to the absorption stays approximately constant with radius to  $R \sim 25 \text{ kpc}$  (Dickey et al. 2009). This implies that the CNM to WNM mixture can be considered as constant throughout the Galaxy. We have to stress here that the model considerations above represent mostly a static view of the ISM, neglecting dynamical processes. Static models fail to explain CNM gas far out in the Galactic disk.

Within the Galactic disk the pressure is higher, and we observe predominantly neutral clouds that are arranged within filamentary and sheet-like structures (Heiles & Troland 2003, Meyer et al. 2006). Toward volume densities in excess of  $n = 10^2 \text{ cm}^{-3}$  photoionization of neutral carbon exceeds the heating by soft X-rays and its efficiency increases constantly. However, the photoelectric effect is more than an order of magnitude more efficient than the neutral carbon excitation. On the cooling side of the equilibrium equation, the fine-structure transitions of neutral carbon at  $\lambda\lambda 609 \mu\text{m}$  and  $370 \mu\text{m}$  become important but are about an order of magnitude less efficient than the  $\lambda 157.7 \mu\text{m}$  transition.

### 5.3. Physical Conditions of the Neutral Interstellar Medium Traced by H I Observations

Starting from the comprehensive analyses of the LAB survey, we use the Haud & Kalberla (2007) plots to estimate the overall temperature and pressure distribution of the ISM. Their analysis provides observational evidence for two phases of the neutral atomic hydrogen: a cold one with a velocity dispersion  $\Delta v = 4 \text{ km s}^{-1}$  and a warm one with  $\Delta v \simeq 24 \text{ km s}^{-1}$ . Heiles & Troland (2003) found a larger value for the CNM and a smaller one for the WNM, focusing on the H I in the Solar Neighborhood.

In the following, we will use the Haud & Kalberla (2007) values, which represents the whole accessible sky without biasing too much to local effects. Using the equation,

$$T_{\text{kin}} \leq \frac{m_{\text{H}} \Delta v}{8 k \ln 2}, \quad (4)$$

we can estimate the upper limit for the kinetic temperature to 300 K for the CNM and 10,000 K for the WNM. Both phases are frequently observed simultaneously across the whole sky, but do they trace coherent physical structures? The answer is certainly yes for high Galactic altitude clouds, IVCs, and HVC complexes, but for low altitudes this answer has to be reconsidered critically.

First, we estimate the so-called size-linewidth relation to estimate the linear size of the gaseous phases. The size-linewidth relation assumes that, proportional to the length of the line of sight through a gas layer, the H I emission line grows in line width. To apply this relation we have to use a “normalization factor” denoted as  $\sigma(1)$  in literature. Following Wolfire et al. (2003),  $\sigma_{\text{CNM}}(1) = 1.2 \text{ km s}^{-1}$ ,  $\sigma_{\text{WNM}}(1) = 1.4 \text{ km s}^{-1}$ , and

$$d = \left( \frac{\sigma}{\sigma(1)} \right)^{\frac{1}{q}}, \quad (5)$$

where  $\sigma$  denotes the FWHM of the Gaussian line that approximates the observed H I emission line. This gives  $\sigma_{\text{CNM}} = \frac{4 \text{ km s}^{-1}}{2\sqrt{2} \ln 2} \simeq 1.6 \text{ km s}^{-1}$  and  $\sigma_{\text{WNM}} = 9.4 \text{ km s}^{-1}$ .  $q = 0.33$  (Larson 1981) is a frequently used parameter over a length range from 1 to 1000 pc (see Wolfire et al. 2003). We find as a rough estimate for the relevant linear extent  $d_{\text{CNM}} \sim 3 \text{ pc}$  for the CNM and  $d_{\text{WNM}} \sim 660 \text{ pc}$  for the WNM. In the case of the CNM, we can safely denote coherent structures in position, velocity, and temperatures as “clouds”, whereas the WNM structures appear to cover linear scales comparable to the scale height of the warm gas distribution (see Section 3.2.2). Toward low Galactic latitudes and, in particular, toward the inner Galaxy the line of sight passes multiple WNM cells, whereas toward high Galactic latitudes the number of WNM turbulence cells is low and local effects dominate.

We conclude that within the plane of the Milky Way CNM clouds are mostly embedded within a bath of WNM gas. This picture has two important implications. The CNM has a much lower volume and area filling factor than the WNM, and the density contrast between the spiral-arm and interarm regions is low because of the large size of the WNM structures in comparison to their separation.

Now we focus on cooling time and volume densities. Theoretically, we can estimate the cooling time of both gaseous phases by:

$$t_{\text{cool}} = \frac{5}{2} \frac{1.1 n k T}{n^2 \Lambda}, \quad (6)$$

where  $n$  is the volume density of all hydrogen species  $n = n_{\text{HI}} + n_{\text{H}^+} + 2n_{\text{H}_2}$ . Considering low Galactic altitude clouds with neutral hydrogen column densities of  $N_{\text{HI}} \leq 1 \cdot 10^{20} \text{ cm}^{-2}$ , we can safely assume that  $n \simeq n_{\text{HI}}$ . Inserting  $\Lambda = 6 \cdot 10^{-26} \text{ ergs s}^{-1} \text{ cm}^{-3} \times \left( \frac{T}{10,000 \text{ K}} \right)^{0.8}$  (Wolfire et al. 2003) yields

$$t_{\text{cool}} \simeq 460 \text{ yr} \frac{T[\text{K}]}{n[\text{cm}^{-3}]}. \quad (7)$$

With

$$n_{\text{CNM}} = \frac{N_{\text{HI}}(\text{CNM})}{d_{\text{CNM}}} \simeq \frac{1 \cdot 10^{20} \text{ cm}^{-2}}{d_{\text{CNM}}} = 5.4 \text{ cm}^{-3} \quad (8)$$

and  $T_{\text{CNM}} = 300 \text{ K}$ , we find  $t_{\text{cool}}(\text{CNM}) = 1.4 \cdot 10^5 \text{ year}$ . For the WNM we find with  $N_{\text{HI}} = 2 \cdot 10^{20} \text{ cm}^{-2}$  an average volume density of  $n_{\text{WNM}} = 0.1 \text{ cm}^{-3}$ . This yields a cooling time of  $t_{\text{cool}}(\text{WNM}) = 4.6 \cdot 10^7 \text{ year}$ . Obviously, the CNM cools quickly, whereas the WNM needs about

two orders of magnitudes longer. The sound crossing time for the CNM,  $t_s(\text{CNM}) \simeq 2 \cdot 10^6$  year and WNM  $t_s(\text{CNM}) \simeq 7 \cdot 10^7$  year differ also by an order of magnitude. So the CNM relaxes much more quickly than the WNM.

These internal timescales should be compared with those that are relevant for heating on large scales, which can mainly be attributed to the frequency of supernova events within the plane of the Milky Way. Wolfire et al. (2003) estimated the temporal separation between subsequent shocks to  $t_{\text{shock}} \simeq 5.3 \cdot 10^6$  year. Thus, the WNM close to the stellar disk is not expected to be observed in any kind of equilibrium, while the CNM may reach quickly a pressure equilibrium with its environment. This implies that we observe frequently CNM gas embedded within WNM gas. Pressure distortions within the WNM will lead to density fluctuations that may form on timescales of a few  $10^5$  years CNM cores within the WNM cell.

Using the numbers above for the volume densities and the upper limits for the kinetic temperature of the gas, we can estimate the thermal pressure of the CNM to  $P_{\text{CNM}}/k \simeq 1600 \text{ cm}^{-3} \text{ K}$  and for the WNM  $P_{\text{WNM}}/k \simeq 1000 \text{ cm}^{-3} \text{ K}$ . Both are rough estimates but differ by less than a factor of two. Jenkins & Tripp (2007) determined a very accurate value of  $2700 \text{ cm}^{-3} \text{ K}$  for the thermal pressure by studying the fine-structure level population of carbon. Consistent with the discussion above, Jenkins & Tripp (2007) pointed out that changes in thermal pressure occur on small scales. Using the carbon data, they constrain the size of the cooling cores to about 50 AU. The cooling occurs on timescales much shorter than the thermal equilibrium timescale.

In summary, the often assumed thermal pressure equilibrium is an oversimplification of the observed situation. The physical conditions within the clouds are very different but it is likely, because of the very different cooling timescales, we can observe CNM filaments and sheets associated with WNM gas with comparable bulk velocities. The CNM filaments or CNM cores are formed within the WNM because of density distortions. The cooling occurs first on linear scales of a few tens of astronomical units forming multiple cores. When cooling, these cores assemble to filaments or sheets on scales of a few parsecs and timescales of  $10^5$  years. Accordingly, CNM clouds can be considered to be in pressure equilibrium within the ambient WNM.

The gaseous WNM structures have typical sizes of about 600 pc, comparable to the observed scale height of the gas layer. The large extent of these WNM cells and, more important, the long cooling time [ $t_{\text{cool.}}(\text{WNM}) \sim 10 \times t_{\text{shock}}(\text{SNR})$ ] imply for the WNM a small volume density contrast between spiral arms and interarm regions. Here, we assume four spiral arms and shock excitation of the WNM by density waves every  $\sim 10^8$  years, which is  $2 \times t_{\text{cool.}}(\text{WNM})$ .

#### 5.4. Two H I Phases in a Turbulent Flow

Following the discussion above, it is common to assume some kind of equilibrium, mostly dominated by thermal effects. This allows the determination of column densities and the thermal pressure. Within a limited range of pressure  $P_{\text{max}} < 3 \times P_{\text{min}}$ , with  $P_{\text{min}} \simeq 2000 \text{ K cm}^{-3}$  (Heiles 2007), a two phase cloudy structure is formed consisting of a cold core and an envelope of warm neutral gas. At first glance, this picture appears to describe the observed situation well, consistent with the best values of the relevant physical parameters for heating and cooling (Wolfire et al. 1995a, 1995b, 2003). However, H I-line data show increasing evidence that this picture needs to be revised.

Accurate temperatures and volume densities of H I clouds need to be determined by absorption measurements (Dickey & Lockman 1990). Using a sufficiently strong background source beyond the H I cloud, the excitation temperature can be derived from on-source absorption profiles in comparison with off-source positions that define the expected background emission. In the most

simple two-component case we observe

$$T_B = T_S(1 - e^{-\tau}) + T_{bg}e^{-\tau}. \quad (9)$$

Here,  $T_S$  is the spin temperature of the cloud with an optical depth  $\tau$ .  $T_{bg}$  is the background temperature, which is observable without the cloud in the foreground, and we neglect additional foreground H I emission. To resolve cloud structures, high sensitivity and high resolution are needed. A combination of an interferometer with a large single-dish is most appropriate to separate the clumpy CNM from the diffuse background (Kalberla, Schwarz & Goss 1985). From such analyses, the evidence emerged that there is not the expected separation in a cold and warm phase. The most recent observations with the Arecibo telescope (Heiles 2001, Heiles & Troland 2003) show unambiguously that 50% of the gas is located in the “unstable region” of the phase diagram.

Numerical investigations incorporating turbulence and other nonthermal effects suggest that, in agreement with these observational findings, a considerable fraction of the H I gas is transient (Vázquez-Semadeni, Gazol & Scalo 2000; Gazol et al. 2001). The nonlinear development of a thermal instability generates turbulence, which in turn affects the initial flow. The two phases get strongly mixed, and the turbulent motions induce transitions of the gas to the unstable range. These effects get more pronounced for stronger turbulence. Transitions into the unstable range, driving, in particular, gas into the cold phase, should be important whenever the kinetic energy exceeds the thermal energy. Perhaps turbulence can explain the findings of Dickey et al. (2009) that the CNM/WNM mixture remains nearly constant to  $R \sim 25$  kpc.

**5.4.1. Warm and cold gas at high galactic altitudes.** Outside the plane of the disk, for  $z > 100$  pc, the composition of the neutral hydrogen gas is different. Far from the stellar disk, the metallicity of the dominant WNM gas and the dust content is lower. The low metallicities lower the cooling efficiency of the gas, while the lower dust content lowers the heating efficiency. High Galactic altitude clouds are exposed to the extragalactic radiation field and the radiation of the Galactic X-ray halo (Pietz et al. 1998, Kerp et al. 1999), which itself ionizes very efficiently the low volume density regions by their soft X-ray radiation. This is because the photoelectric absorption cross section  $\sigma$  of the ISM is a strong function of the photon energy with  $\sigma \propto E^{-\frac{3}{2}}$  (Wilms et al. 2000). The Milky Way halo gas with a plasma temperature around  $T \simeq 10^{6.15}$  K ionizes the neutral gas much more efficiently than the steep power-law spectrum of the extragalactic X-ray background. Above photon energies of 280 eV, metals dominate the photoelectric absorption, whereas below this carbon K-shell ionization level hydrogen and helium are the main photoelectric absorbers (Wilms et al. 2000).

**5.4.2. Column density structure of high galactic altitude clouds.** Neutral clouds within the disk-halo interface ( $z \sim 1$ -2 kpc) show up with cold cores and warm enveloping gas. This two-phase structure is observed toward all IVCs and the bulk of the HVCs (Kalberla & Haud 2006, Haud 2008). Cores have on average larger infall velocities than envelopes. HVCs, in comparison to IVCs, not only have higher velocities but are also smaller and have fainter cores. Their envelopes show also a larger velocity dispersion (Haud 2008).

The gaseous disk-halo interface differs from the two-phase structure discussed in the previous Section. The “rims” of the HVCs with distances of at least a few kiloparsecs are not characterized by sharp cut-offs of the column density distribution at a certain column density threshold, as shown, e.g., by Brüns et al. (2005) for the Magellanic Stream and Leading Arm. This is consistent with the finding that the average X-ray photon spectrum rises steeply with increasing X-ray photon energy (Gilli, Comastri & Hasinger 2007). The steep rise of the extragalactic X-ray spectrum to high X-ray photon energies yields a deficit of soft X-ray photons. These are, however, the most

efficient ionizing photons ( $E < 0.28$  keV) and are dominantly produced in the Milky Way halo with a vertical scale height of about 4 kpc (Kalberla 2003). Accordingly, close to or within the gaseous distribution of the Milky Way X-ray halo, we observe a well-defined neutral column density threshold of about  $N_{\text{HI}} \sim 10^{19} \text{ cm}^{-2}$ , whereas at larger distances from the Galactic X-ray halo plasma, low neutral hydrogen column densities of about  $N_{\text{HI}} \sim 10^{17} \text{ cm}^{-2}$  can be observed (Braun & Thilker 2005).

**5.4.3. Heating and cooling of high galactic altitude clouds.** All HVC complexes, with the only exception of HVC complex L, contain subunits showing a head-tail morphology (Brüns et al. 2000). These HVCs are characterized by a cometary shape, and the head is always associated with a CNM core. The tail consists entirely of WNM gas. The CNM in the head has always a more extreme velocity than the tail, which appears to trail the head. The prototype of a head-tail HVC is HVC 125 + 41-207 (Brüns, Kerp & Pagels 2001). Using radio interferometric data, Braun & Burton (2000) discovered an extremely dense CNM core with a peak brightness temperature of 75 K. This is consistent with the assumption that the head-tail structures are found toward HVCs, which interact with the gaseous Milky Way halo or the intergalactic matter (Brüns et al. 2000). The narrow line width of less than  $2.47 \text{ km s}^{-1}$  and the high column density in excess of  $N_{\text{HI}} = 4 \cdot 10^{20} \text{ cm}^{-2}$  suggest undercool gas. Follow-up searches for  $^{12}\text{CO}$  ( $1 \rightarrow 0$ ) failed (C. Brüns, priv. comm.), suggesting that the CNM head cools very efficiently only because of its expected high volume density. Ram-pressure interaction induces density distortions in the HVC gas, forming dense and cool cores. Also consistent with this scenario is that the WNM gas of the tail has an increased turbulent velocity dispersion toward the rims of the total gas distribution.

The observational results clearly demonstrate that HVCs are accreted by the gravitational potential of the Milky Way galaxy and interact with the gaseous environment. Many HVCs substructures and compact HVCs (CHVCs) show a cometary morphology (e.g., Brüns et al. 2000, Brüns & Westmeier 2004, Ben Bekhti et al. 2006, Peek et al. 2007). Hydrodynamical simulations of HVCs moving through a diffuse hot gaseous component imply that the external medium must have a density greater than  $10^{-4} \text{ cm}^{-3}$  (Quilis & Moore 2001, Peek et al. 2007).

**5.4.4. High-velocity clouds in the disk-halo interface.** At more modest velocities, some of the HVC lines appear to “connect” to the Milky Way HI distribution at lower velocities. Pietz et al. (1996) searched systematically the Leiden-Dwingeloo survey for faint HI emission. After a careful evaluation of the stray radiation contribution to the HI spectra, so-called velocity bridges were detected toward some of the major HVC complexes. Most of these bridges are associated with excess soft X-ray emission (Kerp et al. 1998). Kerp & Pietz (1998) pointed out that the observed excess soft X-ray emission must be a product of enhanced cooling. Toward the rims of the HVCs, the volume density increases by ram-pressure and leads to an increase in the volume density and eventually in the emission measure ( $EM \propto n_e^2$ ). Thus, the compression leads to enhanced cooling and not, as naively expected, to a heating of the HVC boundary (Kerp, Lesch & Mack 1994).

Heating is inefficient because the sound speed in the HIM as well as the Alfvén speed ( $\sim 140 \text{ km s}^{-1}$ ) are comparable to the bulk velocity of the HVC gas. Strong shocks between the HVC and halo plasma are not expected in the interaction zone, but a significant enhancement of the volume density is. The compression zone will first be detectable in emission in the X-ray regime with a mean photon energy of 0.15 keV, corresponding to the plasma temperature of  $T \simeq 10^{6.15} \text{ K}$ . Because of the high cooling efficiency in this photon energy range, the gas cools to  $T \simeq 10^5 \text{ K}$  until the cooling efficiency gets low. The interaction zone is then detectable in UV and in optical absorption line measurements of highly ionized species. Fox, Savage & Wakker

(2006) find, from the analysis of 63 extragalactic lines of sight, evidence for a spatial displacement between the neutral HVC gas and the highly ionized species. They suggest that the HI of the HVCs exists in a separate lower temperature phase than the observed OVI gas. Depending on the local conditions of the compression zone (mainly determined by the volume density), the interface region between the HVC and the HIM is expected to appear very patchy.

**5.4.5. Thermal equilibrium of HI clumps in the disk-halo interface.** Two regions with halo clumps in the outer part of the Milky Way have been mapped at high resolution (Dedes 2008). These clumps belong to a larger sample with properties typical for the clump population discussed in Section 3.2.1. Distances were estimated from the rotation curve to  $13 \lesssim R \lesssim 15$  kpc and  $2.5 \lesssim |z| \lesssim 4$  kpc. Effelsberg spectra show in both cases a pronounced two-phase structure with a cold HI core and an extended warm envelope, but at 9 arcmin resolution the clumps appear to be unresolved. At high angular resolution, obtained by VLA and WSRT observations, the cores fragment into a number of clumps with typical sizes of 2–5 pc. These cores are found to have pressures that are close to the pressures estimated for the HI envelopes. From the Bonn halo model (Pietz et al. 1998, Kalberla & Dedes 2008) there is, in addition, a pressure equilibrium with a surrounding HIM.

Individual clumps appear to be arranged in groups with a filamentary structure. Within such a group the center velocities of individual clumps differ by no more than the mean FWHM linewidths. The pressures of individual clumps show random fluctuations of 25% to 40%, but this is close to the expected observational uncertainties. **Figure 12** shows the location of clumps and cores within the Wolfire et al. (2003) phase diagram. The clumps have temperatures of  $150 \lesssim T_{\text{kin}} \lesssim 700$  K, indicating that they are transient. The HI envelope protects the clumps from evaporation but the lifetime of the clumps is in the range of 0.4 to 0.8 Myears.

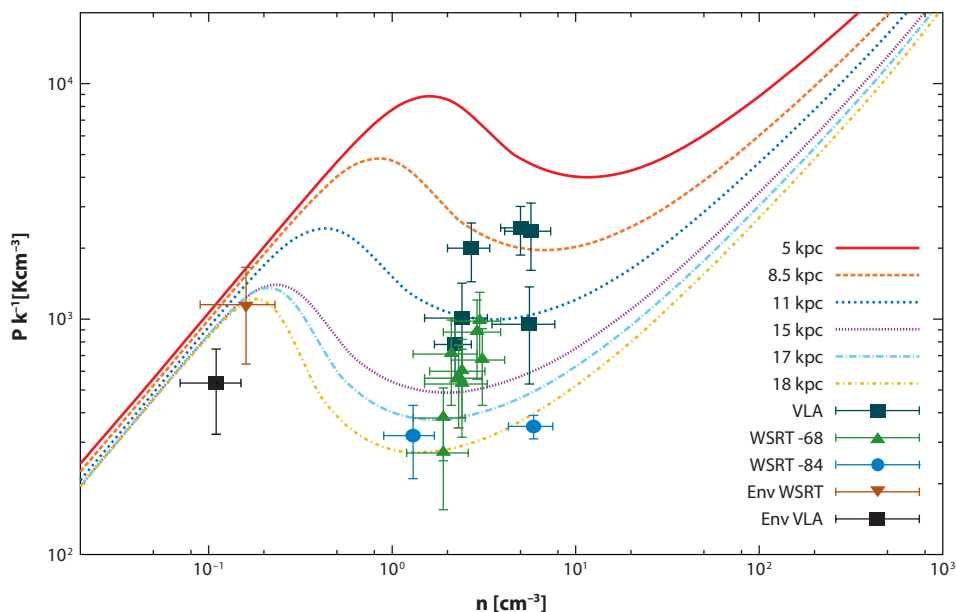


**Figure 12**

Pressure versus volume density for HI halo clumps and envelopes (Env) at  $13 \lesssim R \lesssim 15$  kpc and  $2.5 \lesssim |z| \lesssim 4$  kpc (Dedes 2008). The kinetic temperatures of the clumps are in the range of  $150 \lesssim T_{\text{kin}} \lesssim 700$  K. The Figure was kindly provided by L. Dedes.

This example shows that single-dish observations, in this case with a 100-m telescope, may have insufficient angular resolution to resolve internal cloud structures. Arecibo data at  $R \sim 12$  kpc and  $z \sim 1.4$  kpc led to comparable results as plotted in **Figure 12**, but with a somewhat larger scatter.

Only a few H I halo clumps have been studied in detail, but these suggest that H I halo clumps are transient phenomena. The investigations by Stanimirović et al. (2006) and Dedes (2008) show that these clouds also exist in the outer Milky Way. The detection probability is only 50% lower than for the more extensively studied regions in the inner part of the Milky Way. Taking into account that the investigations by Lockman (2002b) and Ford et al. (2008) were located in regions with active star formation, the high detection rate toward the outskirts of the Milky Way is quite unexpected.

**5.4.6. Tiny-scale atomic structures.** First evidence for tiny-scale atomic structures came from VLBI observations. Such structures, on scales of a few astronomical units to  $\sim 200$  AU, seem to represent a special form of the CNM (Heiles 1997). Column densities of such structures are in the range of  $N_{\text{HI}} = 3 \cdot 10^{18} \text{ cm}^{-2}$  to  $N_{\text{HI}} = 2 \cdot 10^{19} \text{ cm}^{-2}$ .

Empirically, it is established that CNM clouds have a typical column density of about  $N_{\text{HI}} = 5 \cdot 10^{19} \text{ cm}^{-2}$  (Heiles & Troland 2003). Recently, a surprising new class of tiny H I clouds has been detected with peak column densities of  $N_{\text{HI}} \lesssim 3 \cdot 10^{18} \text{ cm}^{-2}$ , which is orders of magnitude below this limit. Some clouds were mapped by Braun & Kanekar (2005) during Westerbork absorption-line studies. Until today, about 20 tiny H I features are known (Stanimirović, Heiles & Kanekar 2007); the big surprise is that toward 22 lines of sight without previously known H I absorption, 18 detections were possible with deeper integrations.

The surface filling factor of this new class of tiny clouds appears to be high, however they host only a few percent of the total gas mass. The absorption line data indicate that the column densities are low and the emission lines are very narrow,  $\Delta v \simeq 2 \text{ km s}^{-1}$  (FWHM). This proves that these clouds are cold objects. Moreover, the number of clouds within a certain column density interval follows a  $N^{-1}$  distribution. Accordingly, tiny H I clouds can be considered as the low column density extension of the CNM clouds. The inferred size of these low column density clouds is about 1000–4000 AU. With respect to their linear extent and their volume densities, these tiny structures are nonstable objects in the ISM. Different formation scenarios are under debate, which range from conductive interfaces between CNM and WNM, interstellar turbulence, and shock front interactions with the CNM (Heiles 2007). All these processes are working on the same timescale as the equilibrium timescale of the ISM.

**5.4.7. Cold H I gas.** The Galactic plane surveys provide high-resolution maps of the Galactic plane, which allow new insights in the structure of the ISM. One of the most spectacular results are HISA features like the ones visible in **Figure 13** (Gibson et al. 2000, 2007). HISA structures are observable only in front of an extended and luminous background, in this case caused predominantly by H I line emission from the WNM. Equation 9 implies that only cold gas is observable this way,  $T_S < T_{\text{bg}}$ , but the advantage is that extended CNM gas clouds are easily recognizable; their distribution can be compared with CO maps. **Figure 13** shows a slice through the Perseus arm; the disk is about 100 pc thick and HISA filaments are visible throughout.

Gibson et al. (2000, 2005) find temperatures  $T_S \sim 70$  K and densities  $n \sim 60 \text{ cm}^{-3}$  in the Perseus arm. Some features are unresolved, implying diameters of  $\lesssim 0.6$  pc. There is partly a correlation between CNM and molecular gas but the majority of the HISA features have no obvious  $^{12}\text{CO}$  counterparts (see **Figure 13**). In the local arm, it is possible to see even colder gas,  $T_S \sim 40$  K, and densities of  $n \sim 120 \text{ cm}^{-3}$ . HISA in the inner Galaxy is better correlated with  $^{12}\text{CO}$  emission (Kavars et al. 2005); H I temperatures and densities approach typical values of dense molecular gas.

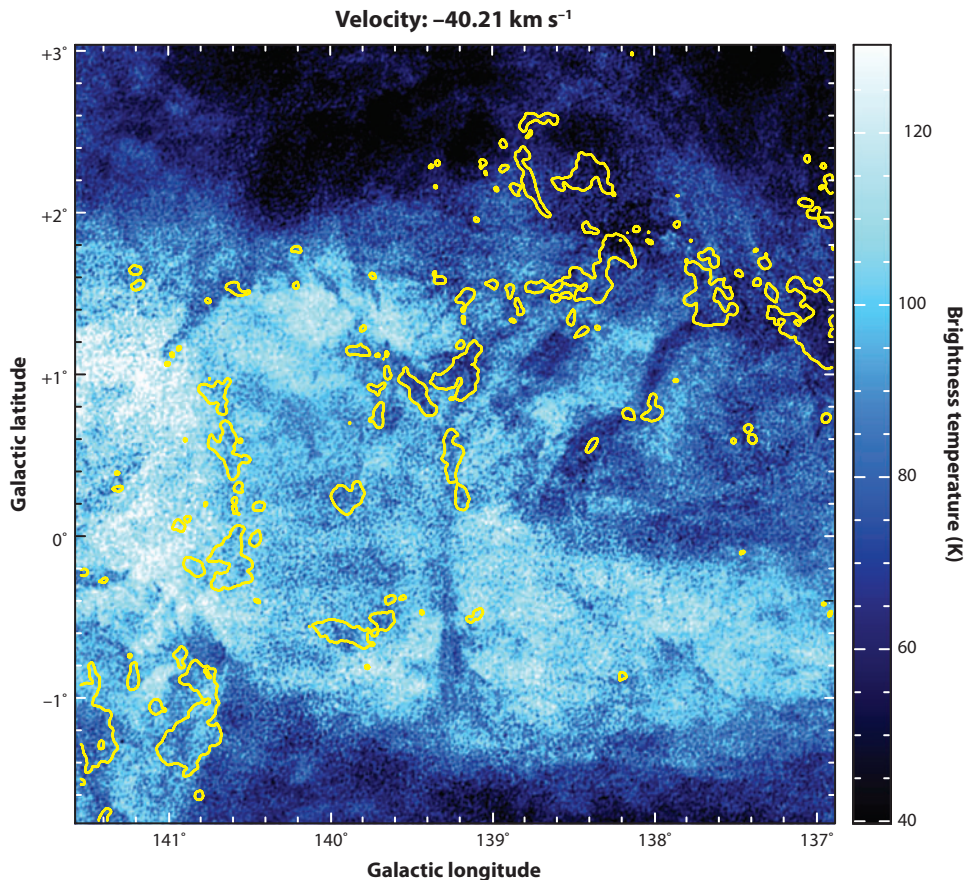


**Figure 13**

Sample of HI self-absorption features within the Galactic plane from the Canadian Galactic Plane Survey (Gibson et al. 2000, 2007). Cold HI gas shows up in absorption against the extended WNM background. Superposed are yellow contours for CO emission (Heyer et al. 1998). The gas is located at a distance of  $\sim 2$  kpc and belongs to the Perseus spiral arm. The Figure was kindly provided by S. Gibson.

Evidence for cold CNM gas was reported also by Dickey et al. (2003) from the SGPS. They find a median temperature of 65 K. Clouds at temperatures of 40 K are common, but most of the CNM is warmer (40–100 K). Heiles & Troland (2003), using the Arecibo telescope for absorption measurements against continuum sources, find a similar result. Their CNM temperature diagram peaks at 40 K with a median at 48 K. This sample includes continuum sources at high Galactic latitudes. They find that the local CNM gas for  $|b| > 10^\circ$  does not show significant differences from gas located in the plane of the disk. In summary, the high-resolution survey work within the past decade has shown that very cold HI gas (Knapp & Verschuur 1972) is not that exceptional, as was believed before.

## 6. SUMMARY AND OUTLOOK

We live in a marvelous era for 21-cm astronomy. Within the past decade new surveys and new instruments provided a rich wealth of data with unprecedented quality. These are single-dish

all-sky surveys (LAB: LDS and IAR) as well as interferometer surveys in the Galactic plane (GPS: CGPS, SGPS, and VGPS). As important as the surveys are, it's the sophisticated data processing procedures that led to major improvements in precision and reliability of the available databases. It is a symbiosis of hardware and software that led to major improvements, not to mention many people who dedicated their work to survey projects!

In the near future, even better single-dish surveys will become available. In the first place we mention the Parkes Galactic All Sky Survey (GASS), observed with a 13-beam receiver, covering declinations  $\delta \lesssim 0^\circ$  with a resolution of 16 arcmin. The first release is expected early in 2009. A significantly better resolution of 3.4 arcmin is provided by the Arecibo telescope (GALFA-HI survey) for  $-2^\circ < \delta < +38^\circ$ ; observations are still in progress. Last, and not least, the Effelsberg telescope will survey the northern sky  $\delta > 0^\circ$  with a 7-beam receiver at a resolution of 9 arcmin (EBHIS). The new all-sky surveys will allow significant improvements in sensitivity and resolution, but it needs to be pointed out that older databases like the LAB survey do not get obsolete. RFI contamination or other systematic errors may be detectable only by cross checking different databases. It is essential to have independent databases for comparison!

The major scientific achievements of these fully-sampled HI surveys will be manifold. They will provide the databases that are necessary to compile complete and consistent physical models of the HI in the ISM. Because HI is a unique tracer for the physical conditions of all gaseous phases, it is the key to studying the evolution of the ISM in the Milky Way as a whole. Today, we are still faced with inconsistencies concerning the multiphase structure of the ISM. There is increasing evidence that a significant portion of the interstellar gas is not in a stable equilibrium. The cooler the gas, the quicker it can reach a pressure equilibrium with its environment. However, as demonstrated in Section 5.3, the overall distributed WNM appears to be out of equilibrium almost everywhere across the Milky Way. According to this, observing two or more phases along similar lines of sight at comparable bulk velocities with similar properties does not imply necessarily a physical equilibrium of the observed gaseous phases.

Applying such a dynamical view of the interstellar gas to HVCs, IVCs, and the gas in the Galactic plane appears to be an attractive and physically supported alternative to some of the present-day models of the ISM. The disadvantage of the dynamical view of the ISM is its complexity when focusing on the astronomical unit and parsec scale. Here, dynamical processes are expected to dominate. Only on the largest scales may we average across a variety of physical conditions to derive global equilibrium parameters like temperature, pressure, density, and scale height.

The new Milky Way HI surveys will open for X-ray astronomers a window to the early universe. Future X-ray observatories will have a significant fraction of their detection power in the soft X-ray energy range below 1 keV. The emission of active Galactic nuclei at high redshifts ( $z \sim 10$ ) or the faint emission of clusters of galaxies at moderate redshifts ( $3 \lesssim z \lesssim 5$ ) is shifted to this soft X-ray band. It is not possible to analyze the X-ray data quantitatively without knowing in detail the distribution of the Galactic ISM. This is because of the large photoelectric absorption cross section of the ISM that follows  $\sigma \propto E^{-\frac{8}{3}}$ . The softer the X-ray radiation of interest, the larger the attenuation of the X-rays by the Galactic ISM.

We need to overcome the present situation in which X-ray astronomy is focused predominantly on two low-HI column density windows of the Milky Way. For a better census and to overcome the "cosmic conspiracy," it is necessary to open the whole high Galactic latitude sky to X-ray astronomy. The Parkes and Effelsberg surveys will provide ideal databases to determine quantitatively the distribution of the WNM, which determines mainly the opacity of the ISM for soft X-rays. Only for high Galactic latitude CNM clouds is higher angular resolution necessary to correct for the additional photoelectric absorption.

The detailed knowledge of the column density distribution of the neutral atomic hydrogen of the Milky Way is also essential to disclose the distribution of the dominant fraction of the baryonic matter in the Universe. Following the  $\Lambda$ CDM cosmological model, the bulk of the local baryons is so far undetected. These baryons are expected to belong to the warm-hot intergalactic medium (WHIM) with temperatures of a few  $10^6$  K. The emission of this thin hot plasma is detectable only in the very soft X-ray range below 0.2 keV. Here, photoelectric absorption by the Milky Way ISM absorbs up to 90% of the incident radiation. Only the accurate knowledge of H I column densities allows to correct for this absorption to unravel the distribution of the WHIM plasma, which illuminates the “spider-web” structures connecting the individual clusters of galaxies in the local Universe.

The mapping of the Galactic plane with interferometers is still in progress. Future technological progress is expected from new correlator techniques and focal-plane phased arrays may eventually lead to a major increase of the survey speed. In any case the Square Kilometer Array (SKA) will be a major leap forward, allowing at the same time high resolution and high sensitivity. The technical challenges of present-day radio astronomy make it necessary to establish mitigation strategies with the aim to overcome the pollution of the cosmic signals by RFI. Modern surveys already use some of the technology that is needed in the near future by the SKA.

What are the scientific benefits of these achievements? Improved sensitivity and reliability do not need to be discussed but major breakthroughs are to be expected from increases in spatial resolution. Mapping of the CNM, but also of cloud features located in the Galactic halo, need high spatial resolution. This is also essential if we like to correlate 21-cm maps with optical or infrared observations. Space-based parallax surveys (GAIA) will measure distances out to tens of kiloparsecs, enabling improved distance determinations within the Milky Way for a better understanding of the H I distribution in the Milky Way.

## DISCLOSURE STATEMENT

The authors are not aware of any affiliations, memberships, funding, or financial holdings that might be perceived as affecting the objectivity of this review.

## ACKNOWLEDGMENTS

P.K. acknowledges support from Deutsche Forschungsgemeinschaft, grant KA1265/5, J.K. from grant KE757/7. We thank Leonidas Dedes, Steve Gibson, and Benjamin Winkel for preparing figures for this review, and Butler Burton, Ralf-Jürgen Dettmar, John Dickey, Steve Gibson, Carl Heiles, Snezana Stanimirović, and Tobias Westmeier for a careful reading of the manuscript and constructive criticism.

## LITERATURE CITED

- Bajaja E, Arnal EM, Larrarte JJ, Morras R, Pöppel WGL, Kalberla PMW. 2005. *Astron. Astrophys.* 440:767  
Ben Bekhti N, Brüns C, Kerp J, Westmeier T. 2006. *Astron. Astrophys.* 457:917  
Benz AO, Grigis PC, Hungerbühler V, Meyer H, Monstein C, et al. 2005. *Astron. Astrophys.* 442:767  
Binney J, Dehnen W. 1997. *MNRAS* 287:L5  
Binney J, Merrifield M. 1998. *Galactic Astronomy*. Princeton, NJ: Princeton Univ. Press  
Blitz L, Spergel DN. 1991. *Astrophys. J.* 370:205  
Braun R, Burton WB. 2000. *Astron. Astrophys.* 354:853  
Braun R, Kanekar N. 2005. *Astron. Astrophys.* 436:L53  
Braun R, Thilker DA. 2005. In *Extra-Planar Gas*, ed. R Braun, p. 121. ASP Conf. Proc. 331

- Breitschwerdt D, Freyberg MJ, Truemper J, eds. 1998. *The Local Bubble and Beyond. Lect. Notes Phys.* 506
- Brüns C, Kerp J, Kalberla PMW, Mebold U. 2000. *Astron. Astrophys.* 357:120
- Brüns C, Kerp J, Pagels A. 2001. *Astron. Astrophys.* 370:L26
- Brüns C, Kerp J, Staveley-Smith L, Mebold U, Putman ME, et al. 2005. *Astron. Astrophys.* 432:45
- Brüns C, Westmeier T. 2004. *Astron. Astrophys.* 426:L9
- Burton WB. 1976. *Annu. Rev. Astron. Astrophys.* 14:275
- Burton WB. 1988. See Verschuur & Kellermann 1988, p. 295
- Burton WB. 1992. In *The Galactic Interstellar Medium, Saas-Fee Advance Course 21*, ed. D Pfenniger, P Bartholdi, p. 1. Berlin: Springer-Verlag
- Burton WB, Liszt HS. 1993. *Astron. Astrophys.* 274:765
- Burton WB, te Lintel Hekkert P. 1986. *Astron. Astrophys. Suppl.* 65:427
- Cordes JM, Freire PCC, Lorimer DR, Camilo F, Champion DJ, et al. 2006. *Astrophys. J.* 637:446
- Daigle A, Joncas G, Parizeau M. 2007. *Astrophys. J.* 661:285
- de Avillez MA. 2000. *MNRAS* 315:479
- de Avillez MA, Berry DL. 2001. *MNRAS* 328:708
- Dedes L. 2008. *The cloudy HI halo of the Milky Way*. PhD thesis. Univ. Bonn. Available at [http://hss.ulb.uni-bonn.de/diss\\_online/math\\_nat\\_fak/2008/dedes\\_leonidas](http://hss.ulb.uni-bonn.de/diss_online/math_nat_fak/2008/dedes_leonidas)
- Dickey JM. 2002. In *Single-Dish Radio Astronomy: Techniques and Applications*, ed. S Stanimirovic, D Altschuler, P Goldsmith, C Salter, p. 209. ASP Conf. Proc. 278
- Dickey JM, Lockman FJ. 1990. *Annu. Rev. Astron. Astrophys.* 28:215
- Dickey JM, McClure-Griffiths NM, Gaensler BM, Green AJ. 2003. *Astrophys. J.* 585:801
- Dickey JM, Strasser S, Gaensler BM, Haverkorn M, Kavars D, et al. 2009. *Astrophys. J.* 693:1250
- Diehl R, Halloin H, Kretshmer K, Licht GG, Schönfeld V, et al. 2006. *Nature* 439:45
- Diplas A, Savage BD. 1991. *Astrophys. J.* 377:126
- Ehlerová S, Palouš J. 2005. *Astron. Astrophys.* 437:101
- Ekers RD, Bell JF. 2001. In *Proc. IAU Symp. 196: Preserving the Astronomical Sky, July 1999, Vienna*, ed. RJ Cohen, WT Sullivan, p. 199
- Fich M, Blitz L, Stark AA. 1989. *Astrophys. J.* 342:272
- Ford HA, McClure-Griffiths NM, Lockman FJ, Bailin J, Calabretta MR, et al. 2008. *Astrophys. J.* 688:290
- Fox AJ, Savage BD, Wakker BP. 2006. *Astrophys. J. Suppl.* 165:229
- Fraternali F. 2009. In *Proc. IAU Symp. 254: The Galaxy Disk in Cosmological Context*, ed. J Anderson, J Bland-Hawthorn, B Nordstrom, p. 255
- Fraternali F, Binney JJ. 2008. *MNRAS* 386:935
- Fridman PA. 2008. *Astron. J.* 135:1810
- Gaensler BM, Madsen GJ, Chatterjee S, Mao SA. 2008. *Publ. Astron. Soc. Aust.* 25:184
- Gazol A, Vázquez-Semadeni E, Sánchez-Salcedo FJ, Scalo J. 2001. *Astrophys. J. Lett.* 557:L121
- Gibson SJ, Taylor AR, Higgs LA, Brunt CM, Dewdney PE. 2005. *Astrophys. J.* 626:195
- Gibson SJ, Taylor AR, Higgs LA, Dewdney PE. 2000. *Astrophys. J.* 540:851
- Gibson SJ, Taylor AR, Stil JM, Brunt CM, Kavars DW, Dickey JM. 2007. In *IAU Symp. 237: Triggered Star Formation in a Turbulent ISM, Prague, 2006*, ed. J Palous, BG Elmegreen, p. 363
- Gilli R, Comastri A, Hasinger G. 2007. *Astron. Astrophys.* 463:79
- Giovanelli R. 2008. See Minchin & Momjian 2008, p. 328
- Haffner LM, Reynolds RJ, Tuftle SL, Madsen GJ, Jaehnig KP, Percival JW. 2003. *Astrophys. J. Suppl.* 149:405
- Hartmann D, Burton WB. 1997. *Atlas of Galactic Neutral Hydrogen*. Cambridge, UK: Cambridge Univ. Press
- Hartmann D, Kalberla PMW, Burton WB, Mebold U. 1996. *Astron. Astrophys. Suppl.* 119:115
- Haud U. 2008. *Astron. Astrophys.* 483:461
- Haud U, Kalberla PMW. 2006. *Baltic Astron.* 15:413
- Haud U, Kalberla PMW. 2007. *Astron. Astrophys.* 466:555
- Haverkorn M, Goss WM. 2007. *SINS—Small Ionized and Neutral Structures in the Diffuse Interstellar Medium*. San Francisco: ASP
- Heald GH, Rand RJ, Benjamin RA, Bershady MA. 2007. *Astrophys. J.* 663:933
- Heiles C. 1979. *Astrophys. J.* 229:533

- Heiles C. 1984. *Astrophys. J. Suppl.* 55:585
- Heiles C. 1997. *Astrophys. J.* 481:193
- Heiles C. 2001. *Astrophys. J. Lett.* 551:L105
- Heiles C. 2007. See Haverkorn & Goss 2007, p. 3
- Heiles C, Troland TH. 2003. *Astrophys. J.* 586:1067
- Heithausen A, Brüns C, Kerp J, Weiss A. 2001. In *The Promise of the Herschel Space Observatory*, ed. GL Pilbratt, J Cernicharo, AM Heras, T Prusti, R Harris, ESA-SP 460, p. 431
- Henderson AP, Jackson PD, Kerr FJ. 1982. *Astrophys. J.* 263:116
- Heyer MH, Brunt C, Snell RL, Howe JE, Schloerb FP, Carpenter JM. 1998. *Astrophys. J. Suppl.* 115:241
- Higgs LA, Tapping KF. 2000. *Astron. J.* 120:2471
- Högbom JA. 1974. *Astron. Astrophys. Suppl.* 417(15):426
- Jenkins EB, Tripp TM. 2007. See Haverkorn & Goss 2007, p. 3
- Johnston S, Bailes M, Bartel N, Baugh C, Bietenholz M, et al. 2007. *Publ. Astron. Soc. Aust.* 24:174
- Kalberla PMW. 2003. *Astrophys. J.* 588:805
- Kalberla PMW, Burton WB, Hartmann D, Arnal EM, Bajaja E, et al. 2005. *Astron. Astrophys.* 440:775
- Kalberla PMW, Dedes L. 2008. *Astron. Astrophys.* 487:951
- Kalberla PMW, Dedes L, Kerp J, Haud U. 2007. *Astron. Astrophys.* 469:511
- Kalberla PMW, Haud U. 2006. *Astron. Astrophys.* 455:481
- Kalberla PMW, Mebold U, Reich W. 1980. *Astron. Astrophys.* 82:275
- Kalberla PMW, Schwarz UJ, Goss WM. 1985. *Astron. Astrophys.* 144:27
- Kang J-h, Koo B-C. 2007. *Astrophys. J. Suppl.* 173:85
- Kavars DW, Dickey JM, McClure-Griffiths NM, Gaensler BM, Green AJ. 2005. *Astrophys. J.* 626:887
- Kerp J, Burton WB, Egger R, Freyberg MJ, Hartmann D, et al. 1999. *Astron. Astrophys.* 342:213
- Kerp J, Lesch H, Mack K-H. 1994. *Astron. Astrophys.* 286:L13
- Kerp J, Pietz J. 1998. See Breitschwerdt, Freyberg & Truemper 1998, p. 337
- Kerp J, Pietz J, Kalberla PMW, Burton WB, Egger R, et al. 1998. See Breitschwerdt, Freyberg & Truemper 1998, p. 457
- Kerr FJ. 1962. *MNRAS* 123:327
- Knapp GR, Verschuur GL. 1972. *Astron. J.* 77:717
- Kolpak MA, Jackson JM, Bania TM, Dickey JM. 2002. *Astrophys. J.* 578:868
- Koo B-C, Kang J-h, Salter CJ. 2006. *Astrophys. J. Lett.* 643:L49
- Kuijken K, Gilmore G. 1989. *MNRAS* 239:651
- Kuijken K, Tremaine S. 1994. *Astrophys. J.* 421:178
- Kulkarni SR, Heiles C. 1987. In *Interstellar Processes*, ed. DJ Hollenbach, HA Thronson, p. 87. Dordrecht: Reidel
- Kulkarni SR, Heiles C. 1988. See Verschuur & Kellermann 1988, p. 95
- Larson RB. 1981. *MNRAS* 194:809
- Levine ES, Blitz L, Heiles C. 2006a. *Astrophys. J.* 643:881
- Levine ES, Blitz L, Heiles C. 2006b. *Science* 312:1773
- Levine ES, Heiles C, Blitz L. 2008. *Astrophys. J.* 679:1288
- Lockman FJ. 2002a. In *Seeing Through the Dust: The Detection of HI and the Exploration of the ISM in Galaxies*, ed. AR Taylor, TL Landecker, AG Willis, p. 107. ASP Conf. Ser. 276
- Lockman FJ. 2002b. *Astrophys. J. Lett.* 580:L47
- Lockman FJ, Condon JJ. 2005. *Astron. J.* 129:1968
- Lockman FJ, Gehman CS. 1991. *Astrophys. J.* 382:182
- Lockman FJ, Jahoda K, McCammon D. 1986. *Astrophys. J.* 302:432
- Low FJ, Beintema DA, Gautier TN, Gillett FC, Beichman CA, et al. 1984. *Astrophys. J. Lett.* 278:L19
- McClure-Griffiths NM, Dickey JM, Gaensler BM, Green AJ. 2002. *Astrophys. J.* 578:176
- McClure-Griffiths NM, Dickey JM, Gaensler BM, Green AJ. 2004. *Astrophys. J. Lett.* 607:L127
- McClure-Griffiths NM, Dickey JM, Gaensler BM, Green AJ, Haverkorn M, Strasser S. 2005. *Astrophys. J. Suppl.* 158:178
- McClure-Griffiths NM, Pisano DJ, Calabretta MR, Ford HA, Lockman FJ, et al. 2009. *Ap. J. Suppl.* 181:398
- McKee CF, Ostriker JP. 1977. *Astrophys. J.* 218:148

- Meyer DM, Lauroesch JT, Heiles C, Peek JEG, Engelhorn K. 2006. *Astrophys. J.* 650:L67
- Minchin R, Momjian E, eds. 2008. *The Evolution of Galaxies through the Neutral Hydrogen Window*. AIP Conf. Ser. 1035
- Mock J. 2004. General GALFA Spectrometer Doc. Available at [http://www.naic.edu/alfa/galfa/galfa\\_docs.shtml](http://www.naic.edu/alfa/galfa/galfa_docs.shtml)
- Narayan CA, Saha K, Jog CJ. 2005. *Astron. Astrophys.* 440:523
- Oort JH. 1962. In *The Distribution and Motion of Interstellar Matter in Galaxies*, ed. L Woltjer, p. 71. New York: Benjamin
- Oosterloo T, Fraternali F, Sancisi R. 2007. *Astron. J.* 134:1019
- Peek JEG, Putman ME, McKee CF, Heiles C, Stanimirović S. 2007. *Astrophys. J.* 656:907
- Pidopryhora Y, Lockman FJ, Shields JC. 2007. *Astrophys. J.* 656:928
- Pietz J, Kerp J, Kalberla PMW, Burton WB, Hartmann D, Mebold U. 1998. *Astron. Astrophys.* 332:55
- Pietz J, Kerp J, Kalberla PMW, Mebold U, Burton WB, Hartmann D. 1996. *Astron. Astrophys.* 308:L37
- Prata SW. 1964. *Bull. Astron. Inst. Neth.* 17:511
- Quilis V, Moore B. 2001. *Astrophys. J. Lett.* 555:L95
- Reach WT, Koo B-C, Heiles C. 1994. *Astrophys. J.* 429:672
- Read JI, Lake G, Agertz O, Debattista VP. 2008. *MNRAS* 892:1041
- Richter P, Sembach KR, Howk JC. 2003. *Astron. Astrophys.* 405:1013
- Sánchez-Salcedo FJ, Saha K, Narayan CA. 2008. *MNRAS* 385:1585
- Shane WW. 1967. In *LAU Symp. 31: Radio Astronomy and the Galactic System*, ed. H van Woerden, p. 177. London: Academic
- Simonson SC. 1971. *Astron. Astrophys.* 12:136
- Stanimirović S. 2002. In *Single-Dish Radio Astronomy: Techniques and Applications*, ed. S Stanimirović, D Altschuler, P Goldsmith, C Salter, p. 375. San Francisco: ASP
- Stanimirović S, Heiles C, Kanekar N. 2007. See Haverkorn & Goss 2007, p. 22
- Stanimirović S, Putman M, Heiles C, Peek JEG, Goldsmith PF, et al. 2006. *Astrophys. J.* 653:1210
- Stanko S, Klein B, Kerp J. 2005. *Astron. Astrophys.* 436:391
- Stark AA, Gammie CF, Wilson RW, Bally J, Linke RA, et al. 1992. *Astrophys. J. Suppl.* 79:77
- Staveley-Smith L. 1997. *Publ. Astron. Soc. Aust.* 14:111
- Stil JM, Lockman FJ, Taylor AR, Dickey JM, Kavars DW, et al. 2006a. *Astrophys. J.* 637:366
- Stil JM, Taylor AR, Dickey JM, Kavars DW, Martin PG, et al. 2006b. *Astron. J.* 132:1158
- Strasser S, Taylor AR. 2004. *Astrophys. J.* 603:560
- Taylor AR, Gibson SJ, Peracaula M, Martin PG, Landecker TL, et al. 2003. *Astron. J.* 125:3145
- van Woerden H, Wakker BP, Schwarz UJ, de Boer KS. 2004. *High Velocity Clouds*, ed. H van Woerden, BP Wakker, UJ Schwarz, KS de Boer. *Astrophys. Space Sci. Libr.*, Vol. 312. Dordrecht: Kluwer Acad.
- Vázquez-Semadeni E, Gazol A, Scalo J. 2000. *Astrophys. J.* 540:271
- Verheijen MAW, Oosterloo TA, van Cappellen WA, Bakker L, Ivashina MV, et al. 2008. See Minchin & Momjian 2008, p. 265
- Verschuur GL. 2004. *Astron. J.* 127:394
- Verschuur GL, Kellermann KI, eds. 1988. *Galactic and Extragalactic Radio Astronomy*. Berlin/New York: Springer-Verlag
- Wakker BP. 1991. *Astron. Astrophys.* 250:499
- Wakker BP, van Woerden H. 1997. *Annu. Rev. Astron. Astrophys.* 35:217
- Wilms J, Allen A, McCray R. 2000. *Astrophys. J.* 542:914
- Winkel B, Kerp J, Kalberla PMW, Keller R. 2008. See Minchin & Momjian 2008, p. 259
- Winkel B, Kerp J, Stanko S. 2007. *Astron. Nachr.* 328:68
- Wolfire MG, Hollenbach D, McKee CF, Tielens AGGM, Bakes ELO. 1995a. *Astrophys. J.* 443:152
- Wolfire MG, McKee CF, Hollenbach D, Tielens AGGM. 1995b. *Astrophys. J.* 453:673
- Wolfire MG, McKee CF, Hollenbach D, Tielens AGGM. 2003. *Astrophys. J.* 587:278
- Wouterloot JGA, Brand J, Burton WB, Kwee KK. 1990. *Astron. Astrophys.* 230:21
- York DG, Songaila A, Blades JC, Cowie LL, Morton DC, Wu C-C. 1982. *Astrophys. J.* 255:467



# Contents

An Astronomical Life Salted by Pure Chance <i>Robert P. Kraft</i> .....	1
The H <sub>I</sub> Distribution of the Milky Way <i>Peter M.W. Kalberla and Jürgen Kerp</i> .....	27
Progenitors of Core-Collapse Supernovae <i>Stephen J. Smartt</i> .....	63
Gravitational Waves from Merging Compact Binaries <i>Scott A. Hughes</i> .....	107
Physical Properties and Environments of Nearby Galaxies <i>Michael R. Blanton and John Moustakas</i> .....	159
Hot Subdwarf Stars <i>Ulrich Heber</i> .....	211
High-Contrast Observations in Optical and Infrared Astronomy <i>Ben R. Oppenheimer and Sasha Hinkley</i> .....	253
Magnetic Reconnection in Astrophysical and Laboratory Plasmas <i>Ellen G. Zweibel and Masaaki Yamada</i> .....	291
Magnetic Fields of Nondegenerate Stars <i>J.-F. Donati and J.D. Landstreet</i> .....	333
Star-Formation Histories, Abundances, and Kinematics of Dwarf Galaxies in the Local Group <i>Eline Tolstoy, Vanessa Hill, and Monica Tosi</i> .....	371
Complex Organic Interstellar Molecules <i>Eric Herbst and Erwine F. van Dishoeck</i> .....	427
The Chemical Composition of the Sun <i>Martin Asplund, Nicolas Grevesse, A. Jacques Sauval, and Pat Scott</i> .....	481
Teraelectronvolt Astronomy <i>J.A. Hinton and W. Hofmann</i> .....	523

Gamma-Ray Bursts in the <i>Swift</i> Era <i>N. Gebrels, E. Ramirez-Ruiz, and D.B. Fox</i> .....	567
--	-----

## Indexes

Cumulative Index of Contributing Authors, Volumes 36–47 .....	619
Cumulative Index of Chapter Titles, Volumes 36–47 .....	622

## Errata

An online log of corrections to *Annual Review of Astronomy and Astrophysics* articles may be found at <http://astro.annualreviews.org/errata.shtml>